

SECRET

NASA TM SX-306

NASA TM SX-306



1N-08
380 441

TECHNICAL MEMORANDUM

SX-306

[REDACTED] for the
[REDACTED] U.S. Air Force

PERFORMANCE, STABILITY, AND CONTROL INVESTIGATION AT
MACH NUMBERS FROM 0.60 TO 1.05 OF A MODEL OF THE

"SWALLOW" WITH OUTER WING PANELS SWEEP 75°

WITH AND WITHOUT POWER SIMULATION

By James W. Schmeer and Marlowe D. Cassetti

Langley Research Center
Langley Field, Va.

Declassified by authority of NASA
Classification Change Notices No. 443
Dated ** 6-28-67

[REDACTED]

NATIONAL AERONAUTICS AND SPACE ADMINISTRATION
WASHINGTON

JUN 23 1960

[REDACTED]

1
2
3
4
5
6
7
8
9
10
11
12
13
14
15
16
17
18
19
20
21
22
23
24
25
26
27
28
29
30
31
32
33
34
35
36
37
38
39
40
41
42
43
44
45
46
47
48
49
50
51
52
53
54
55
56
57
58
59
60
61
62
63
64
65
66
67
68
69
70
71
72
73
74
75
76
77
78
79
80
81
82
83
84
85
86
87
88
89
90
91
92
93
94
95
96
97
98
99
100
101
102
103
104
105
106
107
108
109
110
111
112
113
114
115
116
117
118
119
120
121
122
123
124
125
126
127
128
129
130
131
132
133
134
135
136
137
138
139
140
141
142
143
144
145
146
147
148
149
150
151
152
153
154
155
156
157
158
159
160
161
162
163
164
165
166
167
168
169
170
171
172
173
174
175
176
177
178
179
180
181
182
183
184
185
186
187
188
189
190
191
192
193
194
195
196
197
198
199
200
201
202
203
204
205
206
207
208
209
210
211
212
213
214
215
216
217
218
219
220
221
222
223
224
225
226
227
228
229
230
231
232
233
234
235
236
237
238
239
240
241
242
243
244
245
246
247
248
249
250
251
252
253
254
255
256
257
258
259
260
261
262
263
264
265
266
267
268
269
270
271
272
273
274
275
276
277
278
279
280
281
282
283
284
285
286
287
288
289
290
291
292
293
294
295
296
297
298
299
300
301
302
303
304
305
306
307
308
309
310
311
312
313
314
315
316
317
318
319
320
321
322
323
324
325
326
327
328
329
330
331
332
333
334
335
336
337
338
339
340
341
342
343
344
345
346
347
348
349
350
351
352
353
354
355
356
357
358
359
360
361
362
363
364
365
366
367
368
369
370
371
372
373
374
375
376
377
378
379
380
381
382
383
384
385
386
387
388
389
390
391
392
393
394
395
396
397
398
399
400
401
402
403
404
405
406
407
408
409
410
411
412
413
414
415
416
417
418
419
420
421
422
423
424
425
426
427
428
429
430
431
432
433
434
435
436
437
438
439
440
441
442
443
444
445
446
447
448
449
450
451
452
453
454
455
456
457
458
459
460
461
462
463
464
465
466
467
468
469
470
471
472
473
474
475
476
477
478
479
480
481
482
483
484
485
486
487
488
489
490
491
492
493
494
495
496
497
498
499
500
501
502
503
504
505
506
507
508
509
510
511
512
513
514
515
516
517
518
519
520
521
522
523
524
525
526
527
528
529
530
531
532
533
534
535
536
537
538
539
540
541
542
543
544
545
546
547
548
549
550
551
552
553
554
555
556
557
558
559
560
561
562
563
564
565
566
567
568
569
570
571
572
573
574
575
576
577
578
579
580
581
582
583
584
585
586
587
588
589
590
591
592
593
594
595
596
597
598
599
600
601
602
603
604
605
606
607
608
609
610
611
612
613
614
615
616
617
618
619
620
621
622
623
624
625
626
627
628
629
630
631
632
633
634
635
636
637
638
639
640
641
642
643
644
645
646
647
648
649
650
651
652
653
654
655
656
657
658
659
660
661
662
663
664
665
666
667
668
669
670
671
672
673
674
675
676
677
678
679
680
681
682
683
684
685
686
687
688
689
690
691
692
693
694
695
696
697
698
699
700
701
702
703
704
705
706
707
708
709
710
711
712
713
714
715
716
717
718
719
720
721
722
723
724
725
726
727
728
729
730
731
732
733
734
735
736
737
738
739
740
741
742
743
744
745
746
747
748
749
750
751
752
753
754
755
756
757
758
759
760
761
762
763
764
765
766
767
768
769
770
771
772
773
774
775
776
777
778
779
780
781
782
783
784
785
786
787
788
789
790
791
792
793
794
795
796
797
798
799
800
801
802
803
804
805
806
807
808
809
810
811
812
813
814
815
816
817
818
819
820
821
822
823
824
825
826
827
828
829
830
831
832
833
834
835
836
837
838
839
840
841
842
843
844
845
846
847
848
849
850
851
852
853
854
855
856
857
858
859
860
861
862
863
864
865
866
867
868
869
870
871
872
873
874
875
876
877
878
879
880
881
882
883
884
885
886
887
888
889
890
891
892
893
894
895
896
897
898
899
900
901
902
903
904
905
906
907
908
909
910
911
912
913
914
915
916
917
918
919
920
921
922
923
924
925
926
927
928
929
930
931
932
933
934
935
936
937
938
939
940
941
942
943
944
945
946
947
948
949
950
951
952
953
954
955
956
957
958
959
960
961
962
963
964
965
966
967
968
969
970
971
972
973
974
975
976
977
978
979
980
981
982
983
984
985
986
987
988
989
990
991
992
993
994
995
996
997
998
999
1000



SECRET
NATIONAL AERONAUTICS AND SPACE ADMINISTRATION

TECHNICAL MEMORANDUM SX-306

for the

U.S. Air Force

PERFORMANCE, STABILITY, AND CONTROL INVESTIGATION AT

MACH NUMBERS FROM 0.60 TO 1.05 OF A MODEL OF THE

"SWALLOW" WITH OUTER WING PANELS SWEEPED 75°

WITH AND WITHOUT POWER SIMULATION*

By James W. Schmeer and Marlowe D. Cassetti

SUMMARY

An investigation of the performance, stability, and control characteristics of a variable-sweep arrow-wing model with the outer wing panels swept 75° has been conducted in the Langley 16-foot transonic tunnel. Four outboard engines located above and below the wing provided propulsive thrust, and, by deflecting in the pitch direction and rotating in the lateral plane, also produced control forces. The engine nacelles incorporated swept lateral and vertical fins for aerodynamic stability and control. Jet-off data were obtained with flow-through nacelles, simulating inlet flow; jet thrust and hot-jet interference effects were obtained with faired-nose nacelles housing hydrogen peroxide gas generators.

Six-component force and moment data were obtained at Mach numbers from 0.60 to 1.05 through a range of angles of attack and angles of sideslip. Control characteristics were obtained by deflecting the nacelle-fin combinations as elevators, rudders, and ailerons at several fixed angles for each control.

The results indicate that the basic wing-body configuration becomes neutrally stable or unstable at a lift coefficient of 0.15; addition of nacelles with fins delayed instability to a lift coefficient of 0.30. Addition of nacelles to the wing-body configuration increased minimum drag from 0.0058 to 0.0100 at a Mach number of 0.60 and from 0.0080 to

*Title, Confidential.

SECRET


0.0190 at a Mach number of 1.05 with corresponding reductions in maximum lift-drag ratio of 12 percent and 33 percent, respectively. The nacelle-fin combinations were ineffective as longitudinal controls but were adequate as directional and lateral controls. The model with nacelles and fins was directionally and laterally stable; the stability generally increased with increasing lift. Jet interference effects on stability and control characteristics were small but the adverse effects on drag were greater than would be expected for isolated nacelles.

INTRODUCTION

The versatility of a variable-wing-sweep aircraft which combines good low-speed capabilities with good supersonic capabilities would enable such an airplane to accomplish many varied missions. Considerable interest, therefore, has been evinced in determining an airplane configuration having the desired characteristics. The background, development, design concepts, and the advantages claimed for one proposed configuration called the "Swallow" may be found in references 1 and 2. Results of a subsonic investigation including power simulation of the performance, stability, and control characteristics of a model of the Swallow having a wing sweep of 25° are reported in reference 3. Results of wind-tunnel studies of other variable-wing-sweep airplane configurations are available. (For example, see refs. 4 and 5.)

The present investigation, conducted in the Langley 16-foot transonic tunnel, is a continuation of the investigation reported in reference 3. The phase of the investigation reported herein utilized the same 1/12-scale model of the Swallow but with a wing sweep of 75° , corresponding to a high-speed flight configuration. As was the case in reference 3, the performance, stability, and control characteristics of the model were determined both with and without power simulation. Two nacelle configurations were investigated: airflow nacelles which simulated the engine inlet flow, and jet nacelles with faired inlets which provided simulation of jet thrust and permitted evaluation of the jet interference effects.

Tests were conducted at Mach numbers from 0.60 to 1.05, at angles of attack from approximately 0° to 15° , and at angles of sideslip from -5° to 10° . Finned-nacelle deflections from 0° to $\pm 7.5^\circ$ in the pitch plane, 0° to -15° differential deflection in the pitch plane, and from -5° to 10° in the lateral plane were set to correspond to airplane elevator, aileron, and rudder deflections, respectively. A hot-jet exhaust was obtained by means of hydrogen peroxide gas generators operating through a range of jet total-pressure ratios from approximately 2.5 to 4.5. The average Reynolds number per foot was approximately 4×10^6 .



COEFFICIENTS AND SYMBOLS

All coefficients are presented for the body axes system except lift and drag which are presented for the stability axes system. The wing area includes the area of both the forewing (fixed portion) and the outer panels. Moments have been taken about a point located at the trailing-edge apex for a wing sweep angle of 80° .

Coefficients

Model with airflow nacelles:

C_D	drag coefficient, $\frac{\text{Drag}}{qS}$
$C_{D,i}$	nacelle internal drag coefficient, $\frac{\text{Internal drag}}{qS}$
$C_{D,o}$	minimum drag coefficient
C_L	lift coefficient, $\frac{\text{Lift}}{qS}$
C_l	rolling-moment coefficient, $\frac{\text{Rolling moment}}{qSb}$
C_m	pitching-moment coefficient, $\frac{\text{Pitching moment}}{qSc_r}$
C_n	yawing-moment coefficient, $\frac{\text{Yawing moment}}{qSb}$
$C_{p,b}$	base pressure coefficient, $\frac{P_b - P}{q}$
C_Y	side-force coefficient, $\frac{\text{Side force}}{qS}$



Model with jet nacelles:

$C_{D,t}$	total drag coefficient	} Model coefficients including components of jet thrust
$C_{L,t}$	total lift coefficient	
$C_{l,t}$	total rolling-moment coefficient	
$C_{m,t}$	total pitching-moment coefficient	
$C_{n,t}$	total yawing-moment coefficient	
$C_{Y,t}$	total side-force coefficient	
$C_{D,j}$	drag coefficient	} Model coefficients with applicable components of jet thrust removed
$C_{L,j}$	lift coefficient	
$C_{l,j}$	rolling-moment coefficient	
$C_{m,j}$	pitching-moment coefficient	
$C_{n,j}$	yawing-moment coefficient	
$C_{Y,j}$	side-force coefficient	
$\Delta C_{D,j}$	interference drag coefficient, $(C_{D,j})_{\text{jets on}} - (C_{D,j})_{\text{jets off}}$	
C_F	jet thrust coefficient, $\frac{F_j}{pA_j}$	

Symbols

A	cross-sectional area, sq ft
A_j	jet-nacelle exit area, sq ft
b	wing span, ft
c	root chord ($\Lambda = 80^\circ$), ft
F_j	jet thrust, lb



- l maximum model length, axial distance from nose to wing tip, 94.75 in.
- M free-stream Mach number
- p free-stream static pressure, lb/sq ft
- P_b base pressure, lb/sq ft
- q free-stream dynamic pressure, lb/sq ft
- r radius, in.
- S wing area ($\Lambda = 75^\circ$), sq ft
- t/c thickness-chord ratio
- x axial distance, in.
- α angle of attack, deg
- β angle of sideslip, positive nose left, deg
- δ nacelle lateral deflection, positive nose right, deg
- θ nacelle pitch deflection, positive nose up, deg
- $\Delta\theta$ nacelle differential deflection in pitch plane, deg
- Λ leading-edge sweep angle of outboard portion of wing, deg
- ϕ meridian angle, deg

Parameters:

- $C_{L\alpha}$ lift-curve slope, per deg
- $C_{L,(L/D)_{max}}$ lift coefficient for maximum lift-drag ratio
- $C_{L\beta}$ effective dihedral parameter, $\frac{\partial C_L}{\partial \beta}$, per deg
- $C_{L\Delta\theta}$ lateral control effectiveness parameter, per deg



$C_{m_{CL}}$	static longitudinal stability parameter, per deg
$C_{m_{\theta}}$	longitudinal control effectiveness parameter, per deg
$C_{n_{\delta}}$	directional control effectiveness parameter, per deg
$C_{n_{\beta}}$	directional stability parameter, $\frac{\partial C_n}{\partial \beta}$, per deg
L/D	lift-drag ratio
$P_{t,j/p}$	jet total-pressure ratio

Subscripts:

L	left
R	right
max	maximum
1	outer
2	inner

MODEL AND APPARATUS

The investigation reported herein was conducted in the Langley 16-foot transonic tunnel. A 1/12-scale version of a 50,000-pound Swallow strike aircraft (ref. 2) was tested with the wings swept back corresponding to a high-speed configuration. A more detailed description of the wing-body combination is found in reference 3. A sketch of the model with outer wing panels swept 75° is shown in figure 1. The wing-body combination was tested without nacelles (fig. 2(a)) and with either airflow nacelles (fig. 2(b)) or hot-jet nacelles.

The four nacelles, which simulated the Bristol turbojet (BE-38) engine nacelles, were located on the wing with the pivot points for lateral control deflection at the 25-percent-chord and 78-percent-semispan stations (for $\Lambda = 80^\circ$). Both the airflow nacelles and the jet nacelles included swept horizontal and vertical finned surfaces. Figure 3 shows a sketch of the airflow and jet nacelle arrangement. The airflow nacelles simulated the flow conditions for the turbojet-engine

nacelle inlets and the jet nacelles simulated the flow conditions for the turbojet-engine nacelle exits. A more detailed discussion of the nacelle simulation is found in reference 3. Longitudinal control was achieved by rotating all nacelles together in the pitch plane and lateral control was achieved by rotating the nacelles differentially in the pitch plane. Rotation of the nacelles together with the pylons in the yaw plane provided directional control. A hydrogen peroxide decomposition chamber, similar to that described in reference 6, was enclosed in the jet nacelles and produced the simulated hot-jet exhaust of the Swallow turbojet engines.

The Swallow was designed to have a smooth area progression with a basic wing sweepback of 80° as shown in figure 4. The area distribution for the present 75° sweep model with and without nacelles is also shown in figure 4. The model fuselage volume was somewhat less than that proposed by Vickers-Armstrongs as is shown in the difference between the two area curves.


Model forces and moments were obtained from an internal six-component strain-gage balance. Nacelle and fuselage base pressures were obtained through manifolded pressure tubes located at the respective bases on all configurations. The total pressures were also obtained in the jet nacelles through a single probe and in the airflow nacelles through a pressure rake as indicated in figure 3. Model angle of attack was obtained from an internal pendulum strain-gage indicator.

TESTS, CORRECTIONS, AND ACCURACY

Tests

Transition was fixed on the wing by means of 1/8-inch-wide bands of size 180 carborundum grain at the $\frac{2}{2}$ -percent-chord station which extended over the full wing span. The grain size was determined by the method discussed in reference 7.

Wing-body configuration alone and with airflow nacelles.- The aerodynamic characteristics of the basic wing-body combination were investigated at Mach numbers of 0.60, 0.80, 0.90, 1.00, and 1.05 at angles of attack from -2° to about 15° . With the nacelles added, the longitudinal control effectiveness was determined at these same Mach numbers and angles of attack with nacelle longitudinal control deflections of $\theta = 0^\circ, \pm 3^\circ,$ and $\pm 7.5^\circ$. For directional control effectiveness, the model with nacelles deflected at $\delta = 0^\circ, \pm 5^\circ,$ and $\pm 10^\circ$ was tested at angles of sideslip of 0° and 5° over a Mach number range from 0.80 to 1.05 and an angle-of-attack range from 0° to 12° .



SECRET

Model with jet nacelles.- In the power-on portion of this investigation, the jet nacelles were operated at jet total-pressure ratios of approximately 1 (jet off), 2.5, 3.5, and 4.5. For the determination of the power-on longitudinal and directional characteristics, the testing was conducted at approximately the same conditions as the power-off tests. Angle of attack, however, was limited to 0° , 4° , and 8° for the longitudinal control tests and to 4° for the directional control portion of this investigation.

A power-on lateral control investigation was made with the nacelles deflected differentially in the pitch plane at angles of $\Delta\theta = 0^\circ$ ($\theta_L = 0^\circ$, $\theta_R = 0^\circ$), $\Delta\theta = 6^\circ$ ($\theta_L = 3^\circ$, $\theta_R = -3^\circ$), and $\Delta\theta = 15^\circ$ ($\theta_L = 7.5^\circ$, $\theta_R = -7.5^\circ$). This portion of the investigation was conducted at Mach numbers of 0.90 and 1.05 and at angles of attack of 0° , 4° , and 8° .

Static tests were performed on each nacelle to determine the variation of thrust coefficient with jet pressure ratio.

Corrections

Wing-body configuration alone and with airflow nacelles.- The force data have been adjusted to free-stream static pressure at the fuselage base and have been corrected for the effects of nacelle internal drag where applicable. No corrections for the base drag on the airflow nacelles were applied since this correction amounted to less than 0.0001 in drag coefficient in all cases. Fuselage base pressure coefficients are presented in figure 5(a), and the average internal drag coefficients for the upper and lower nacelles are shown in figure 5(b).

Model with jet nacelles.- All coefficients have been adjusted to the condition of free-stream static pressure at the fuselage base and at the nacelle annular bases for the jets-on case. The data were further adjusted to the condition of free-stream static pressure acting on the jet exit areas for the jets-off case. Jet-nacelle base pressure coefficients are presented in figure 6(a). Each simulator was statically calibrated in a manner similar to that described in reference 5. The static-jet-thrust calibrations for the jet simulators are given in figure 6(b).

Coefficients for the jet-nacelle configurations are presented in three forms. (See "Symbols" section.) The coefficients with the subscript t include components of the jet thrust. These coefficients are made up of aerodynamic, jet thrust, and jet interference forces. Coefficients with the subscript j represent data with components of the

jet thrust removed. The jet thrust of each nacelle was determined by using measured jet pressure ratios and the static thrust calibrations. These coefficients are made up of the aerodynamic plus jet interference forces. In the case where jet interference effects are apparent, an incremental coefficient is also used. This is the jet interference coefficient obtained by removal of the jet-off aerodynamic value from the jet-on aerodynamic plus jet interference coefficient.

No corrections for wing aeroelastic effects have been included in the data presented. Rolling-moment data have been corrected for small induced effects due to tunnel airflow angularity and model asymmetry by subtracting the rolling-moment coefficients of the wing-body configuration at zero angle of attack and sideslip from the coefficients for the model with nacelles.

Accuracy

The estimated accuracy of the measurements is as follows:

	<u>M = 0.6</u>	<u>M = 1.05</u>
C_D	±0.0005	±0.0003
C_L	±0.005	±0.003
C_l	±0.0023	±0.0012
C_m	±0.0004	±0.0002
C_n	±0.0036	±0.0019
C_Y	±0.0009	±0.0005
C_F	±0.05	±0.05
$C_{p,b}$	±0.007	±0.004
M	±0.005	±0.005
α , deg	±0.1	±0.1
β , deg	±0.2	±0.2
δ and θ , deg	±0.1	±0.1
$P_{t,j}/P$	±0.05	±0.05

RESULTS

The results of the investigation are presented in the following figures:



Power Off

Aerodynamic characteristics:

Wing-body configuration	7
Wing-body configuration plus nacelles	8
Nacelle deflection for longitudinal control	9
Longitudinal control effectiveness	10

Lateral and directional characteristics:

Nacelle deflection for directional control	11
Directional control effectiveness	12
Nacelle deflection for lateral control	13
Lateral and directional stability	14

Power On

Aerodynamic characteristics with nacelles deflected for longitudinal control:

Jet thrust components included	15
Jet thrust components removed	16
Incremental drag due to jet interference	17

Lateral and directional characteristics with nacelles deflected for directional control:

Jet thrust components included	18
Jet thrust components removed	19

Lateral and directional characteristics with nacelles deflected for lateral control:

Jet thrust components included	20
Jet thrust components removed	21

DISCUSSION

Aerodynamic Characteristics, Power Off

Wing-body configuration and effect of undeflected nacelles.— The basic aerodynamic characteristics of the wing-body configuration are presented in figure 7. In general, Mach number appears to have small effect on the variation of angle of attack, drag coefficient, or pitching-moment coefficient with lift coefficient. The longitudinal stability curves are relatively flat and indicate either neutral stability or mild instability at a lift coefficient of about 0.15.

The effects on the aerodynamic characteristics of adding undeflected nacelles to the wing-body configuration are shown in figure 8. The minimum drag coefficient for the wing-body configuration was about 0.0058 subsonically and increased to a maximum value of 0.0080 at $M = 1.05$. Addition of the nacelles increased $C_{D,0}$ to 0.0100 subsonically and the drag rise, which began about 0.1 lower in Mach number, reached a value of 0.0190 (fig. 8(b)). Correspondingly, the nacelles caused a reduction in maximum lift-drag ratio (untrimmed) of about 12 percent at $M = 0.60$ and 33 percent at $M = 1.05$.

It was shown in reference 3 that the addition of nacelles with fins to the model with a leading-edge sweep of 25° caused a small reduction in the longitudinal stability parameter C_{mC_L} , but in the case of the model with $\Lambda = 75^\circ$ (fig. 8(c)), the nacelles increased the value of C_{mC_L} by nearly 80 percent through the Mach number range. Also shown in figure 8(c) is the slight increase in lift-curve slope $C_{L\alpha}$ due to the addition of the nacelles.

Nacelle deflection for longitudinal control.- The aerodynamic characteristics of the model with nacelles deflected in the vertical plane as a pitch-control device are shown in figure 9. In the presentation of the drag polars (fig. 9(b)), only the data for the undeflected nacelles have been faired for the sake of clarity. The slopes of the pitching-moment curves (fig. 9(c)) for the various nacelle pitch deflections are essentially constant at any given Mach number. Also, for the range of test variables presented, the lift coefficient for the onset of instability is nearly constant at a value of 0.30, which is double the value for the wing-body configuration. The elevator-control power parameter $C_{m\theta}$ was obtained at $\theta = 0^\circ$ from figure 10(a) and plotted on figure 10(b). Although $C_{m\theta}$ is approximately doubled by sweeping the wing back from 25° (see ref. 3) to 75° due to the lengthened moment arm, the value at the larger sweep angle is still relatively low. With the maximum nacelle pitch deflection of these tests ($\theta = 7.5^\circ$), the model could be trimmed only up to a lift coefficient of about 0.15.

Lateral and Directional Characteristics, Power Off

Nacelle deflection for directional control.- The lateral and directional characteristics for the model with nacelles deflected for directional control are presented in figure 11. At $\beta = 0^\circ$ the yawing-moment coefficients decreased with increasing lift for either positive or negative deflection; at $\beta = 5^\circ$, C_n generally tended to become more positive for $\delta = 0^\circ$ and to become more positive more rapidly with lift for



SECRET

increasing positive deflections. As indicated in figure 11(a), approximately 5° "rudder" deflection would be required to provide zero yawing moments at $\beta = 5^\circ$. Figure 11(c) indicates that the rolling moments due to rudder deflection were small and erratic at zero sideslip and were nearly independent of rudder deflection at $\beta = 5^\circ$ where the value of C_l increased rapidly with increasing lift coefficient.

The variation of yawing-moment coefficient with rudder deflection (fig. 12(a)) is essentially linear and the slope of rudder control power $C_{n\delta}$, as shown in figure 12(b), is only slightly affected by Mach number. Increasing lift coefficient from 0.20 to 0.40 reduces $C_{n\delta}$ by about 20 to 25 percent through the Mach number range.

Nacelle deflection for lateral control.- The lateral and directional characteristics of the model with airflow nacelles deflected differentially for lateral control were not investigated. However, since the differences between the control characteristics for the airflow-nacelle and the jet-nacelle configurations were found to be trivial, the lateral control effectiveness was obtained from the jet-off points of the jet-nacelle investigation (fig. 20(c)) and plotted in figure 13. At zero angle of attack the aileron control power $C_{l\Delta\theta}$ was found to be 0.00078 and 0.00090 for Mach numbers of 0.90 and 1.05, respectively. The effect of increasing angle of attack was small. The yawing moments due to deflecting the nacelles for roll control were negligible. (See fig. 20(a).)

Stability characteristics.- The lateral and directional stability characteristics are presented in figure 14. The directional stability parameter $C_{n\beta}$ is positive at all test conditions and increases with increasing lift. Generally, $C_{n\beta}$ also increases with Mach number. Rolling moment due to sideslip is zero at zero lift but at lifting conditions the effective dihedral parameter $C_{l\beta}$ is negative. The values increase negatively (increasing positive effective dihedral) with increasing lift but decrease with increasing Mach number especially at the higher lift coefficient.

Aerodynamic Characteristics, Power On

Nacelle deflection for longitudinal control.- The aerodynamic characteristics, including components of the jet thrust, for the model with various deflections of the nacelles for pitch control are presented in figure 15. The relative flatness of the lift and pitching-moment coefficient variation with total pressure ratio indicates little contribution of thrust to either of these components. It is apparent that the lift

component of thrust and the moment arms through which the thrust vectors act are too small to allow any significant gains in pitch control effectiveness over the pure aerodynamic control provided by the nacelles and fins.

An indication of the jet interference effects is shown in figure 16 where the aerodynamic characteristics with the calculated thrust vectors removed are plotted against jet pressure ratio. Again lift and pitching moments were essentially unaffected as indicated by the fact that the jet-on data are nearly identical to the jet-off data ($p_{t,j}/p = 1.0$). Drag, however, does show sizeable effect due to jet operation. The incremental drag (jets on minus jets off) shown in figure 17 indicates rather large adverse jet effects. The magnitudes are much larger than would be expected based on existing data of jet effects on afterbody drag for similar isolated nacelles (ref. 8). Apparently there are additional jet interferences on the adjacent wing, fin, and support-strut surfaces of this configuration.


Lateral and Directional Characteristics, Power On

Nacelle deflection for directional control.- The lateral and directional characteristics, including jet thrust components, for various nacelle deflections for directional control are presented in figure 18. The variation of the yawing-moment coefficients with jet pressure ratio indicates a moderate contribution of jet thrust to the directional control (fig. 18(a)). With the components of the jet thrust removed (fig. 19), the data indicate no significant effects of jet interference. The results with or without the jet thrust vector included are similar for both $\beta = 0^\circ$ and $\beta = 5^\circ$.

Nacelle deflection for lateral control.- The lateral and directional characteristics, including jet thrust components, for various differential nacelle deflections in the pitch plane are presented in figure 20. The contribution of the jet thrust to rolling moments was about what would be calculated from the thrust vector and moment arms of the respective nacelles. Figure 21(c) shows that there was only a slight adverse effect of jet interference. Yawing moment due to roll control deflection was insignificant.

SUMMARY OF RESULTS

An investigation of the performance, stability, and control characteristics of a variable-sweep arrow-wing model with the outer wing panels swept 75° indicates the following results:



SECRET

(1) The basic wing-body configuration exhibited longitudinal instability or neutral stability at a lift coefficient of about 0.15 for all test Mach numbers; the addition of nacelles and fins delayed the onset of instability to a lift coefficient of about 0.30.

(2) The addition of the four nacelles to the basic wing-body configuration increased minimum drag from 0.0058 to 0.0100 subsonically (at a Mach number of 0.60) and from 0.0080 to 0.0190 at a Mach number of 1.05; the maximum lift-drag ratio (untrimmed) was correspondingly reduced by 12 percent and 33 percent, respectively.

(3) The nacelle-fin combinations were ineffective for longitudinal control but appeared to be adequate for directional and lateral control.

(4) The directional stability parameter $C_{n\beta}$ was positive at all test conditions and increased with increasing lift.

(5) Rolling moments due to sideslip were zero at zero lift but at lifting conditions the effective dihedral parameter $C_{l\beta}$ was negative, indicating stability which increased with increasing lift but decreased with Mach number.

(6) The jet interference effects on the model stability and control characteristics were small; the adverse effects on drag were greater than would be expected for isolated nacelles.

(7) For the maximum nacelle pitch deflection of these tests, the contribution of the thrust vectors to pitching-moment control was small.

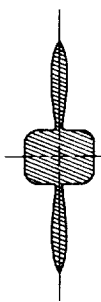
Langley Research Center,
National Aeronautics and Space Administration,
Langley Field, Va., May 16, 1960.



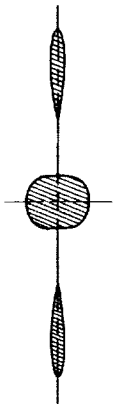
REFERENCES

1. Wallis, B. N.: A Note on a Proposed New Type of Aircraft. Vickers-Armstrongs (Aircraft), Ltd. (Weybridge, England).
2. Anon.: The "Swallow" Project - Proposal for a Research Aircraft Capable of Wide Military Applications (Including Strike Reconnaissance Duties). Preliminary Drawings, Vickers-Armstrongs (Aircraft), Ltd. (Weybridge, England).
3. Runckel, Jack F., Schmeer, James W., and Cassetti, Marlowe D.: Performance, Stability, and Control Investigation at Mach Numbers From 0.4 to 0.9 of a Model of the "Swallow" With Outer Wing Panels Swept 25° With and Without Power Simulation. NASA TM SX-296, 1960.
4. Finch, Thomas W., and Briggs, Donald W.: Preliminary Results of Stability and Control Investigation of the Bell X-5 Research Airplane. NACA RM L52K18b, 1953.
5. Alford, William J., Jr., Luoma, Arvo A., and Henderson, William P.: Wind-Tunnel Studies at Subsonic and Transonic Speeds of a Multiple-Mission Variable-Wing-Sweep Airplane Configuration. NASA TM X-206, 1959.
6. Runckel, Jack F., and Swihart, John M.: A Hydrogen Peroxide Hot-Jet Simulator for Wind-Tunnel Tests of Turbojet-Exit Models. NASA MEMO 1-10-59L, 1959.
7. Braslow, Albert L., and Knox, Eugene C.: Simplified Method for Determination of Critical Height of Distributed Roughness Particles for Boundary-Layer Transition at Mach Numbers From 0 to 5. NACA TN 4363, 1958.
8. Cabbage, James M., Jr.: Jet Effects on the Drag of Conical Afterbodies for Mach Numbers of 0.6 to 1.28. NACA RM L57B21, 1957.

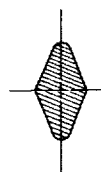
Geometric Characteristics	
Total wing area	6.344 ft ²
Aspect ratio	1.61
Span	38.292 in.
Streamwise t/c	0.036
Airfoil	RAE 102 (t/c = 0.140 perpendicular to L.E.)
Model ref. chord	50 in.
(root chord for $\Lambda = 80^\circ$)	
Moment ref. point	Trailing-edge apex $\Lambda = 80^\circ$



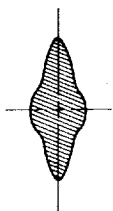
Section A-A
Sta. 20



Section B-B
Sta. 30



Section C-C
Sta. 55



Section D-D
Sta. 65

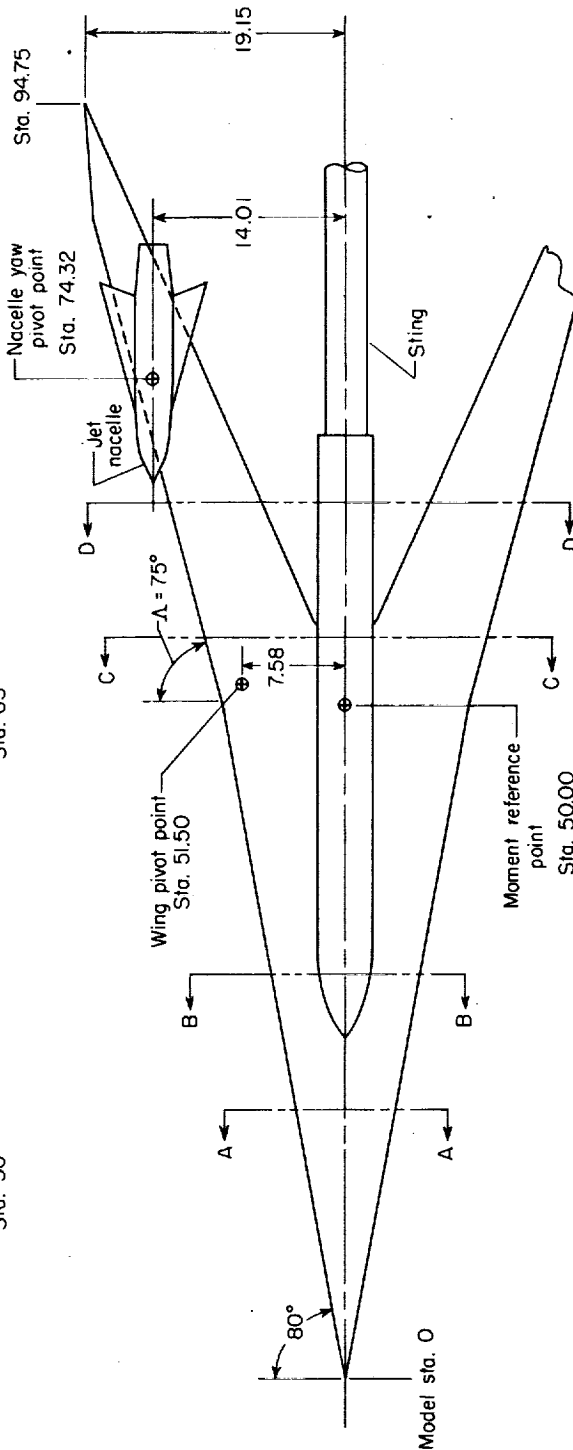


Figure 1.- Sketch of Swallow variable-wing-sweep model. All dimensions are in inches.



(a) Basic wing-body configuration. L-59-4717

Figure 2.- Photographs of model with 75° leading-edge sweep.



(b) Model with airflow nacelles. L-59-4781

Figure 2.- Concluded.

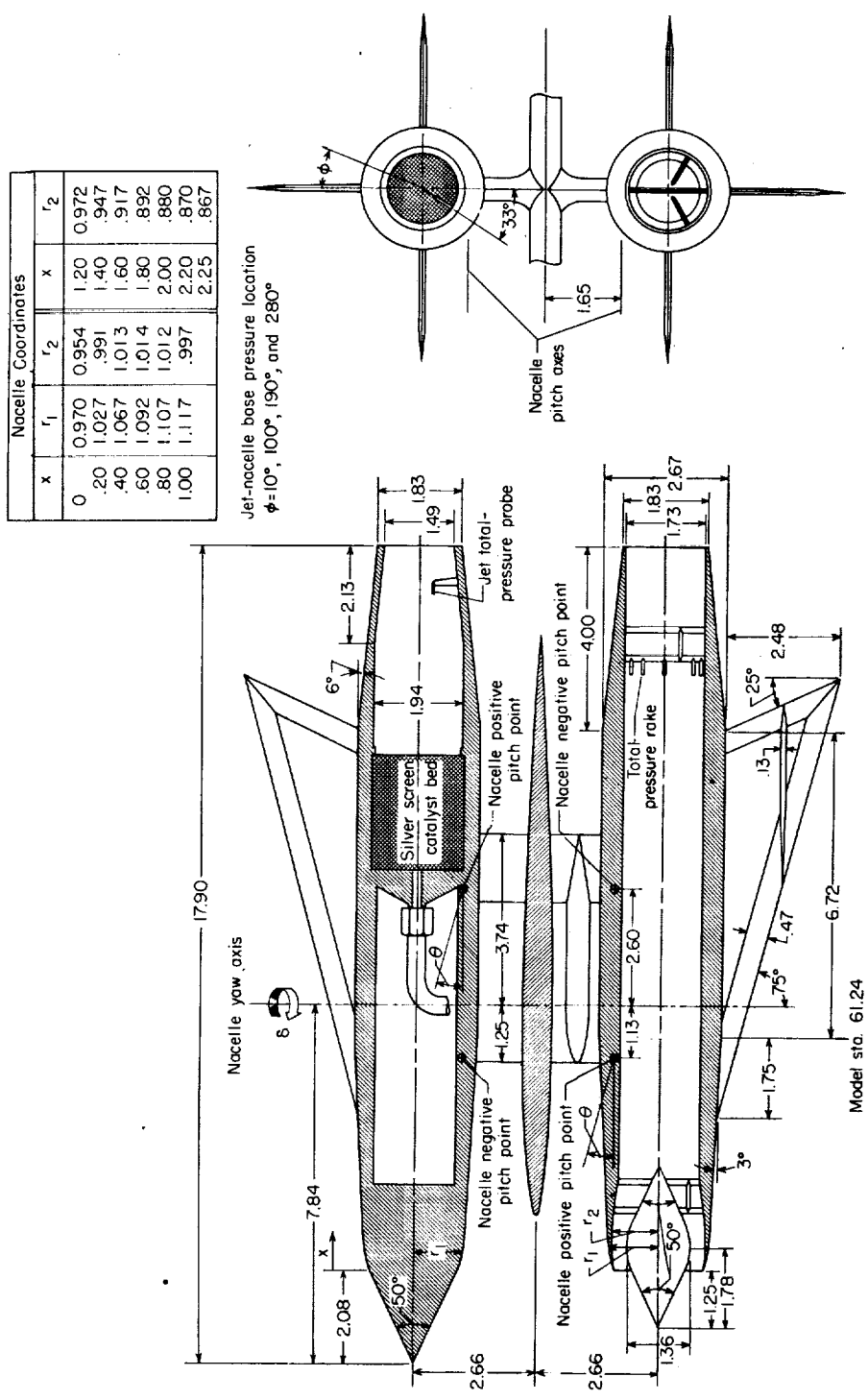


Figure 3.- Sketch showing jet and airflow nacelles, fins, and pylon arrangement. All dimensions are in inches.

SECRET

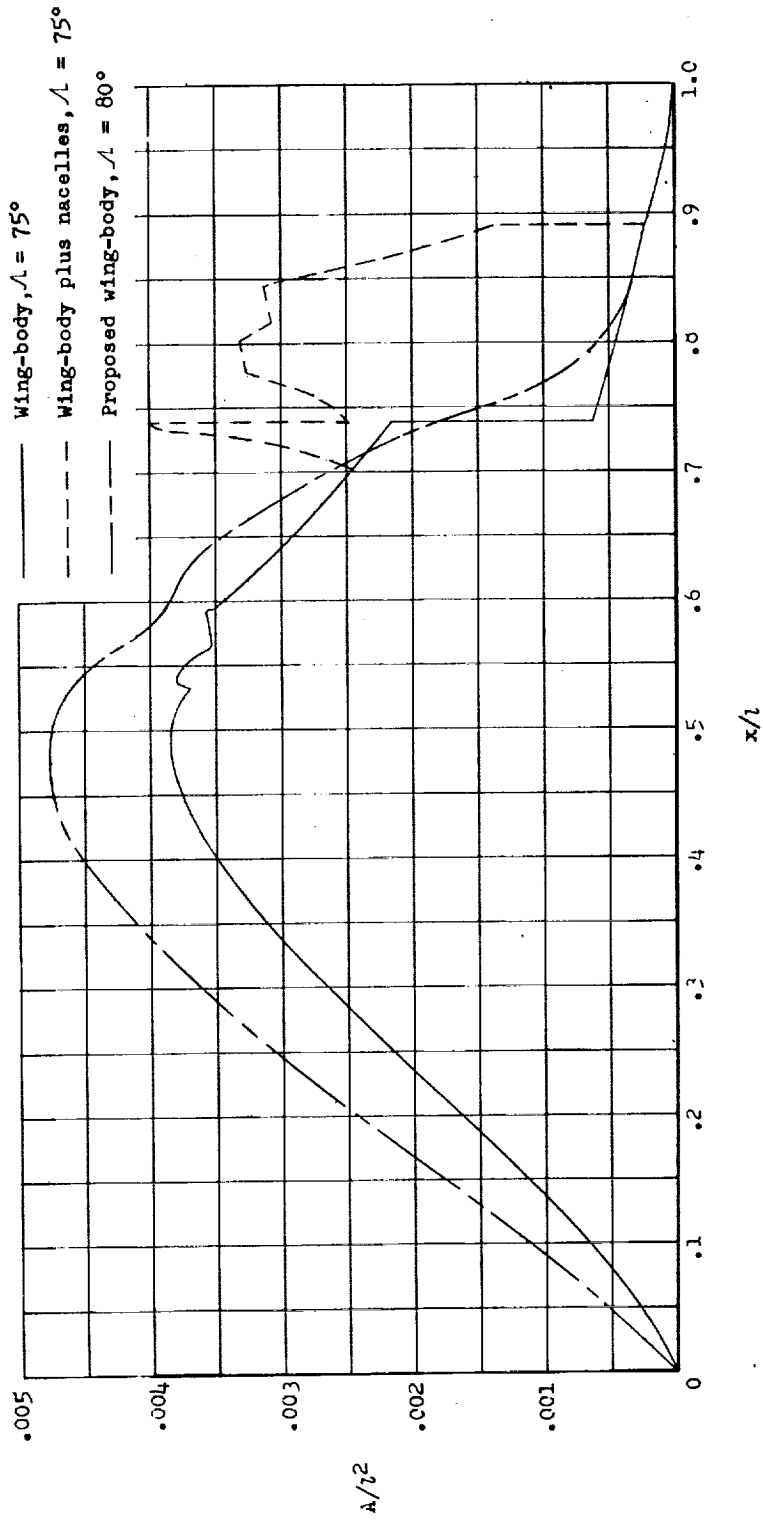
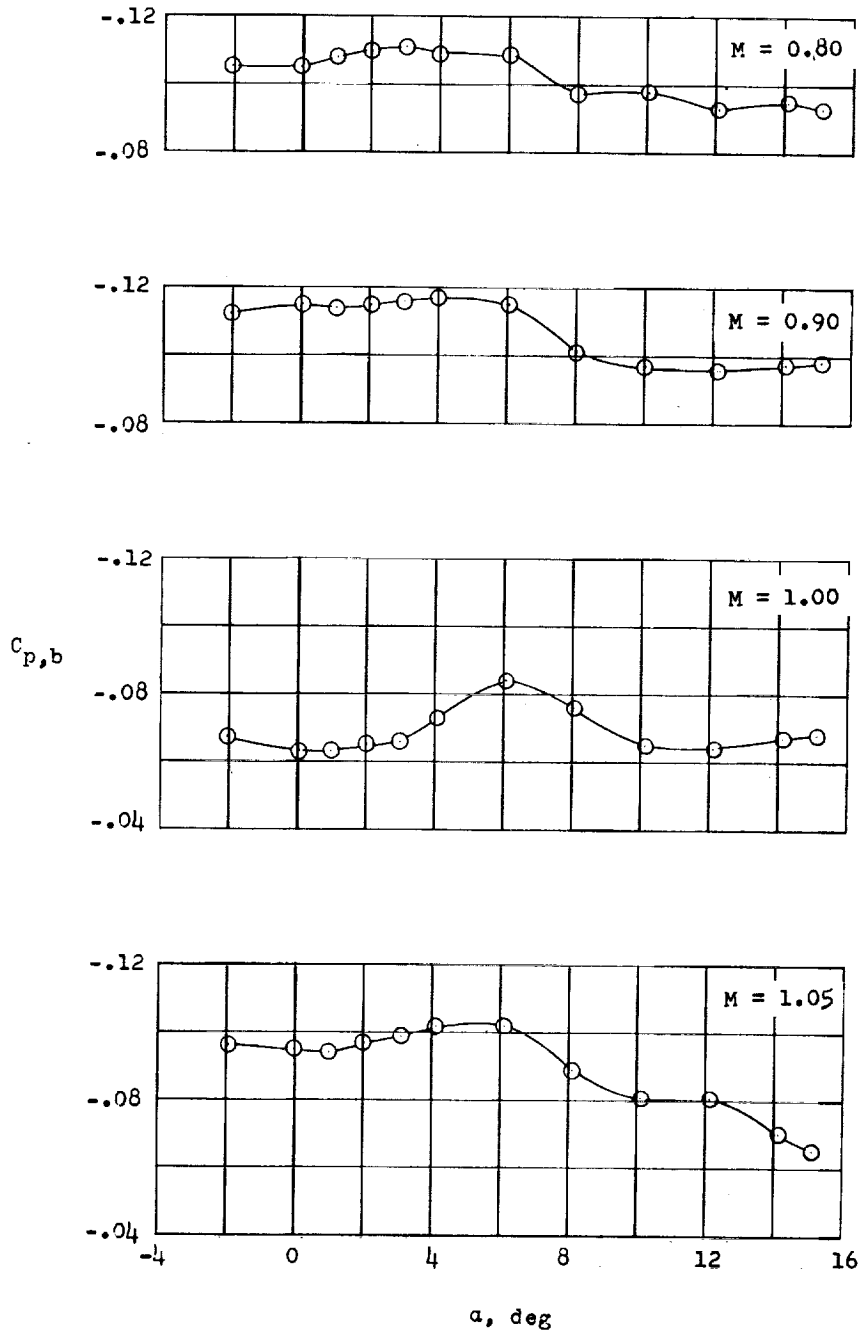


Figure 4.- Area distribution of Swallow variable-wing-sweep model.

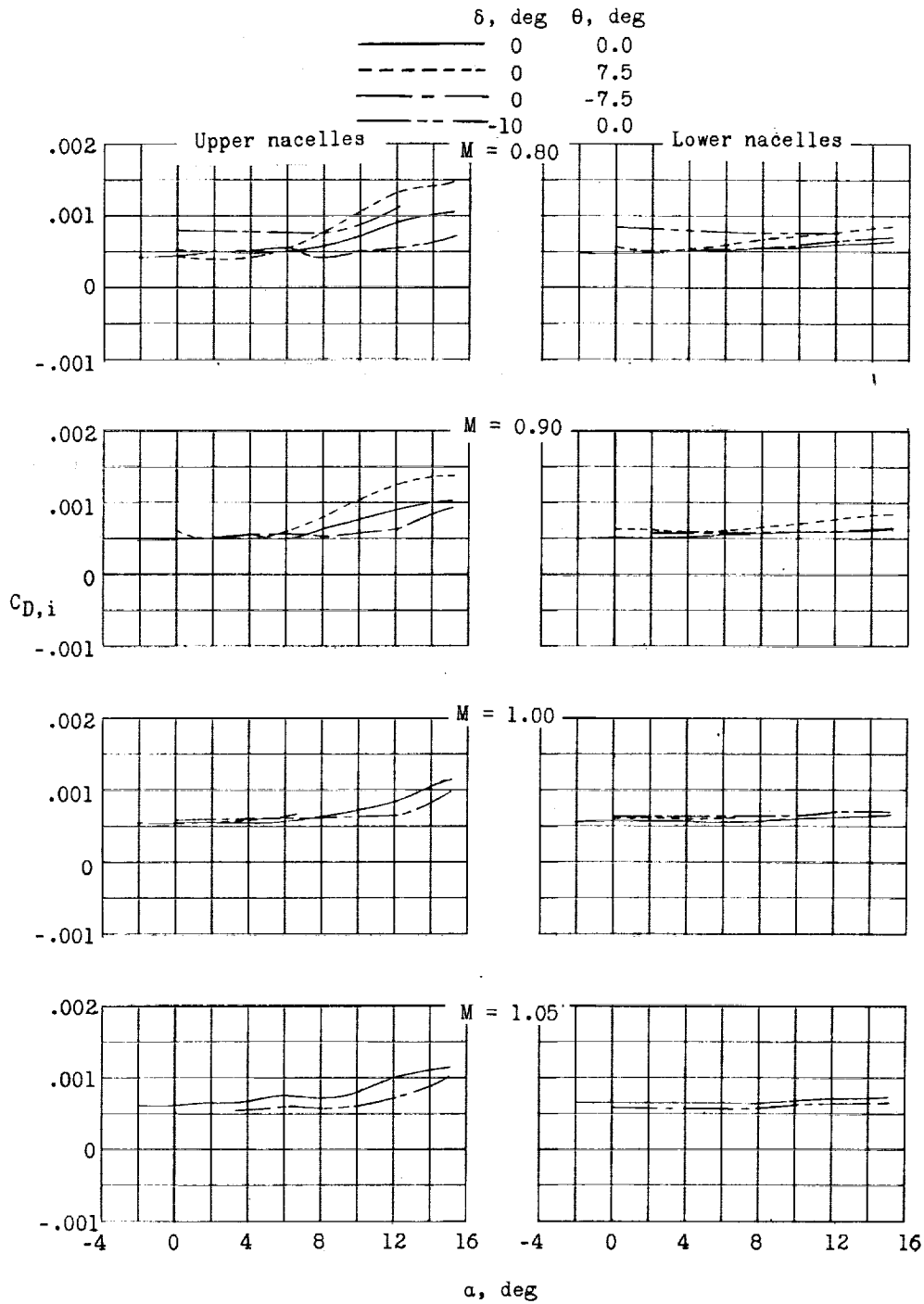


(a) Fuselage base pressure coefficient.

Figure 5.- Fuselage base pressure coefficient and nacelle internal drag coefficient. $\beta = 0^\circ$.

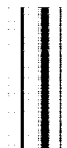


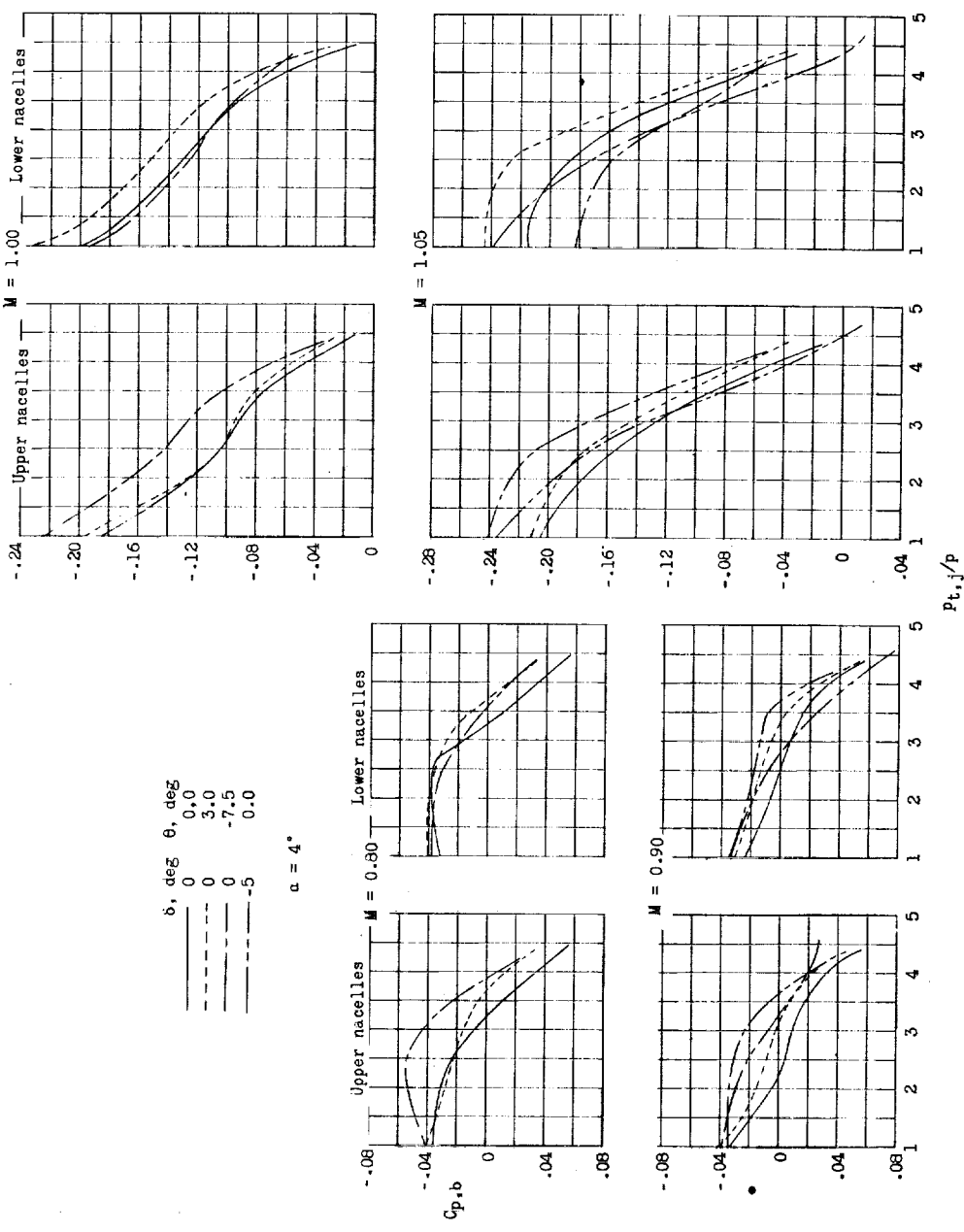
SECRET



(b) Internal drag coefficient.

Figure 5.- Concluded.

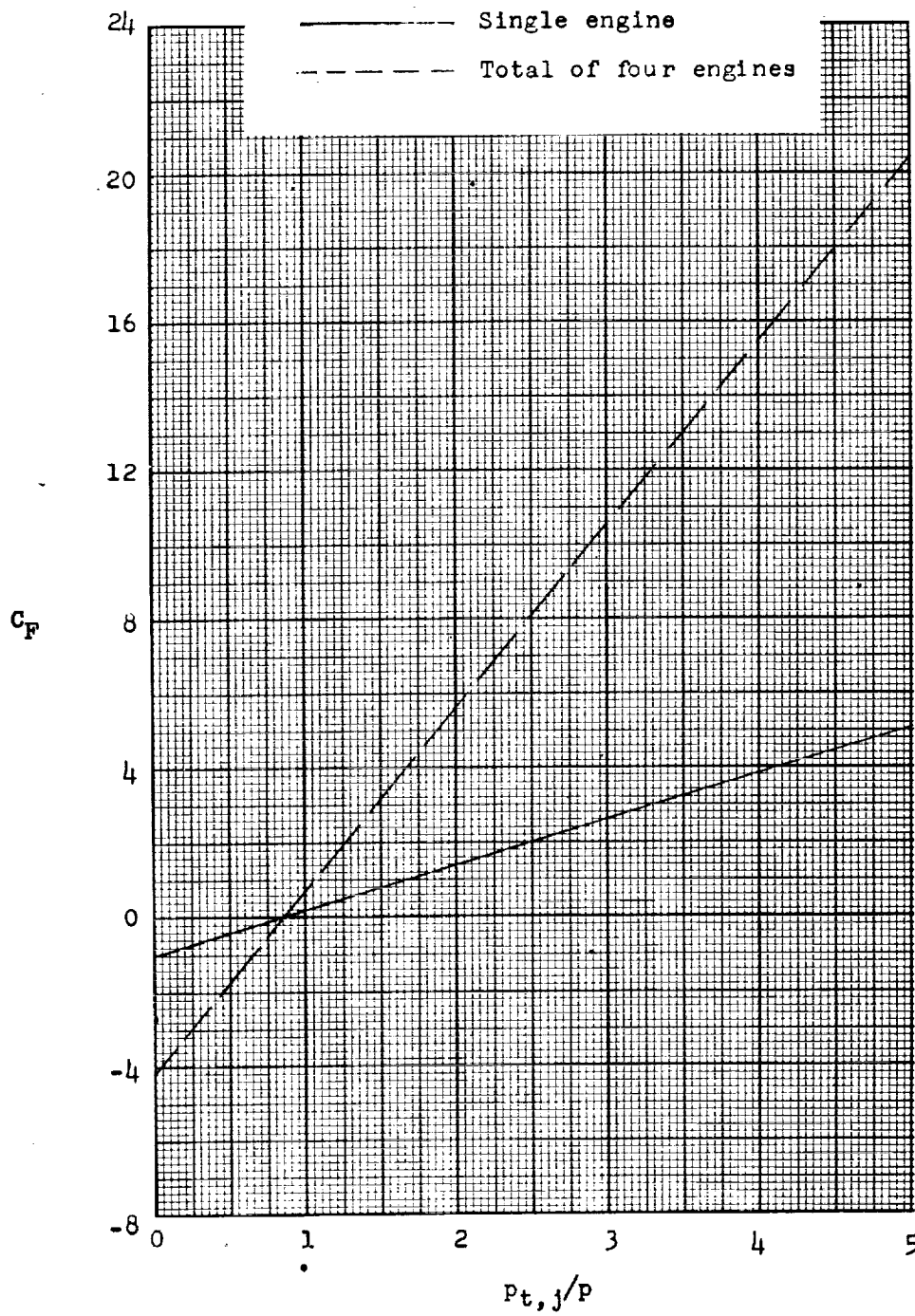




(a) Nacelle base pressure coefficient.

Figure 6.- Nacelle base pressure coefficient and engine static-jet-thrust calibration.

SECRET



(b) Engine static-jet-thrust calibration.

Figure 6.- Concluded.

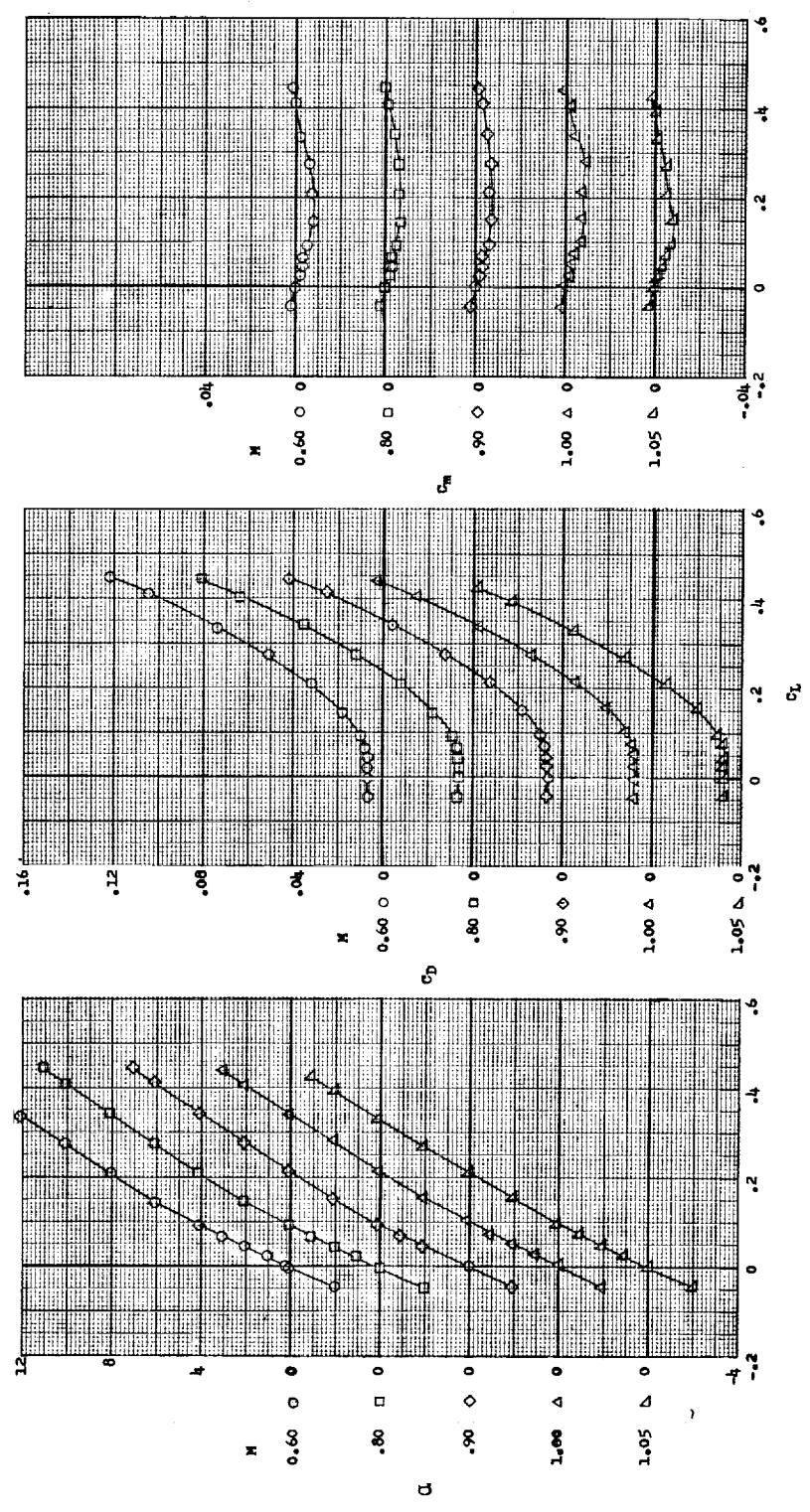
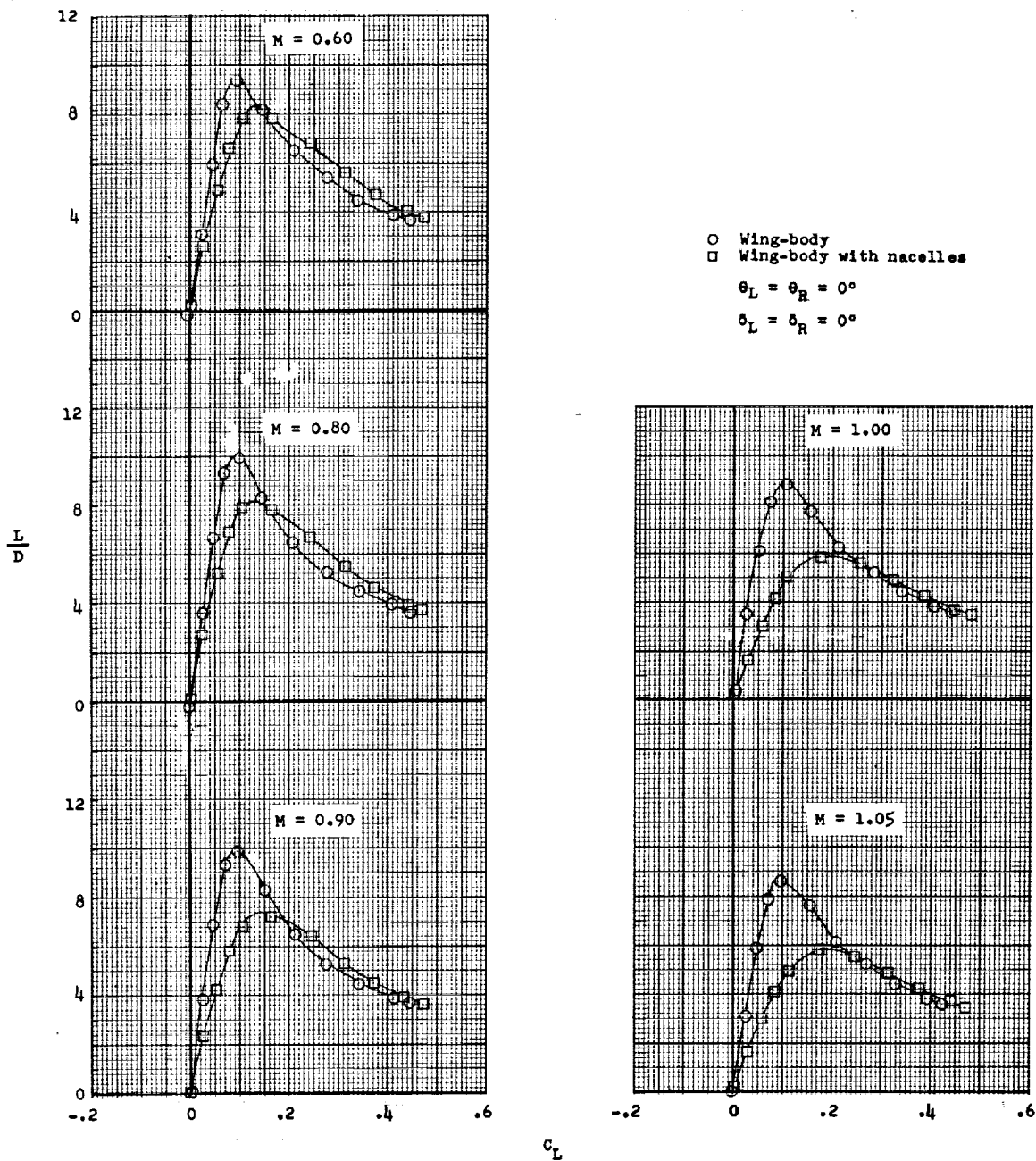
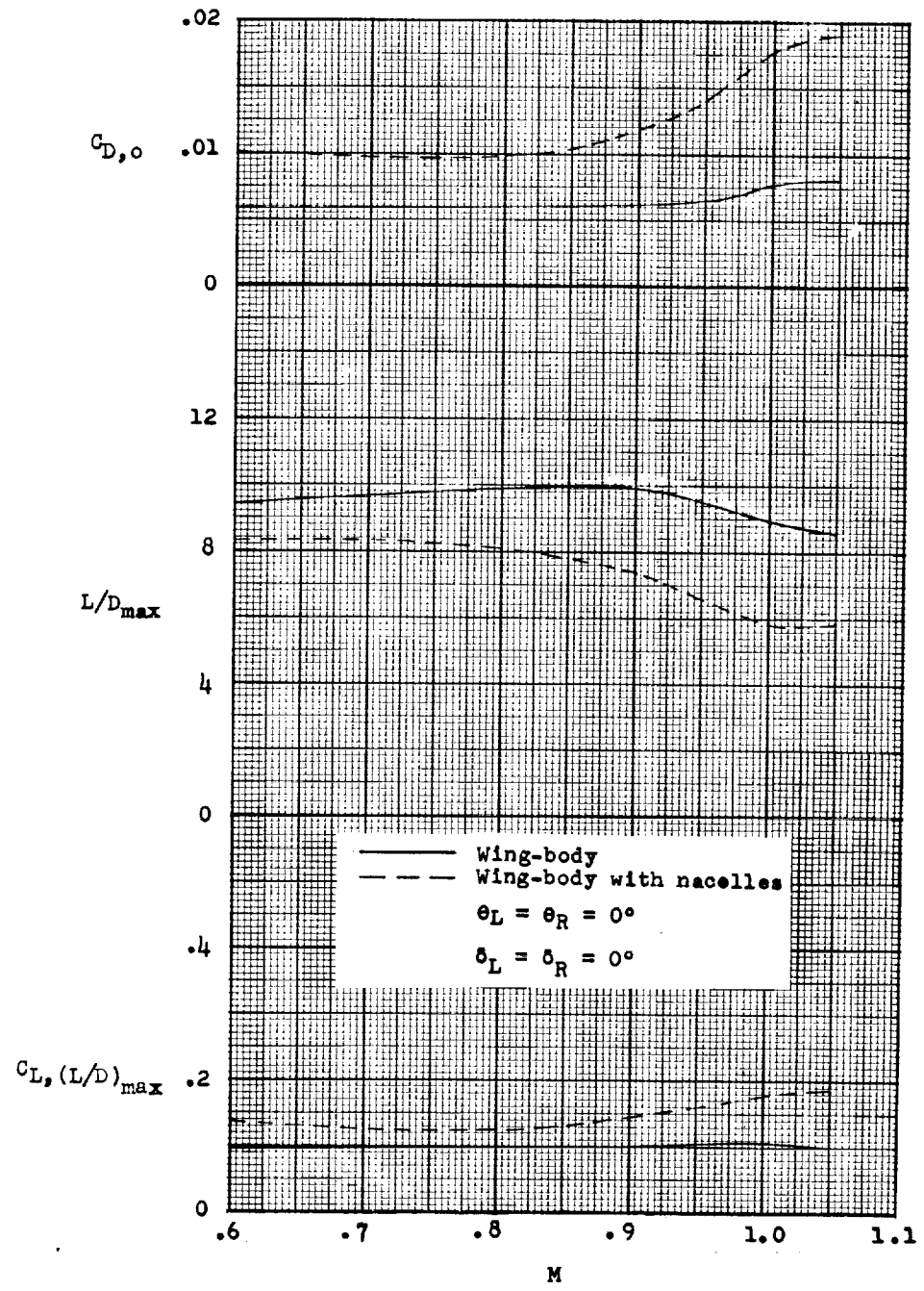


Figure 7.- Aerodynamic characteristics of wing-body configuration. $\Lambda = 75^\circ$; $\beta = 0^\circ$.



(a) Variation of lift-drag ratio with lift coefficient.

Figure 8.- Effect of nacelles on model aerodynamic characteristics.
 $\Lambda = 75^\circ$; $\beta = 0^\circ$.

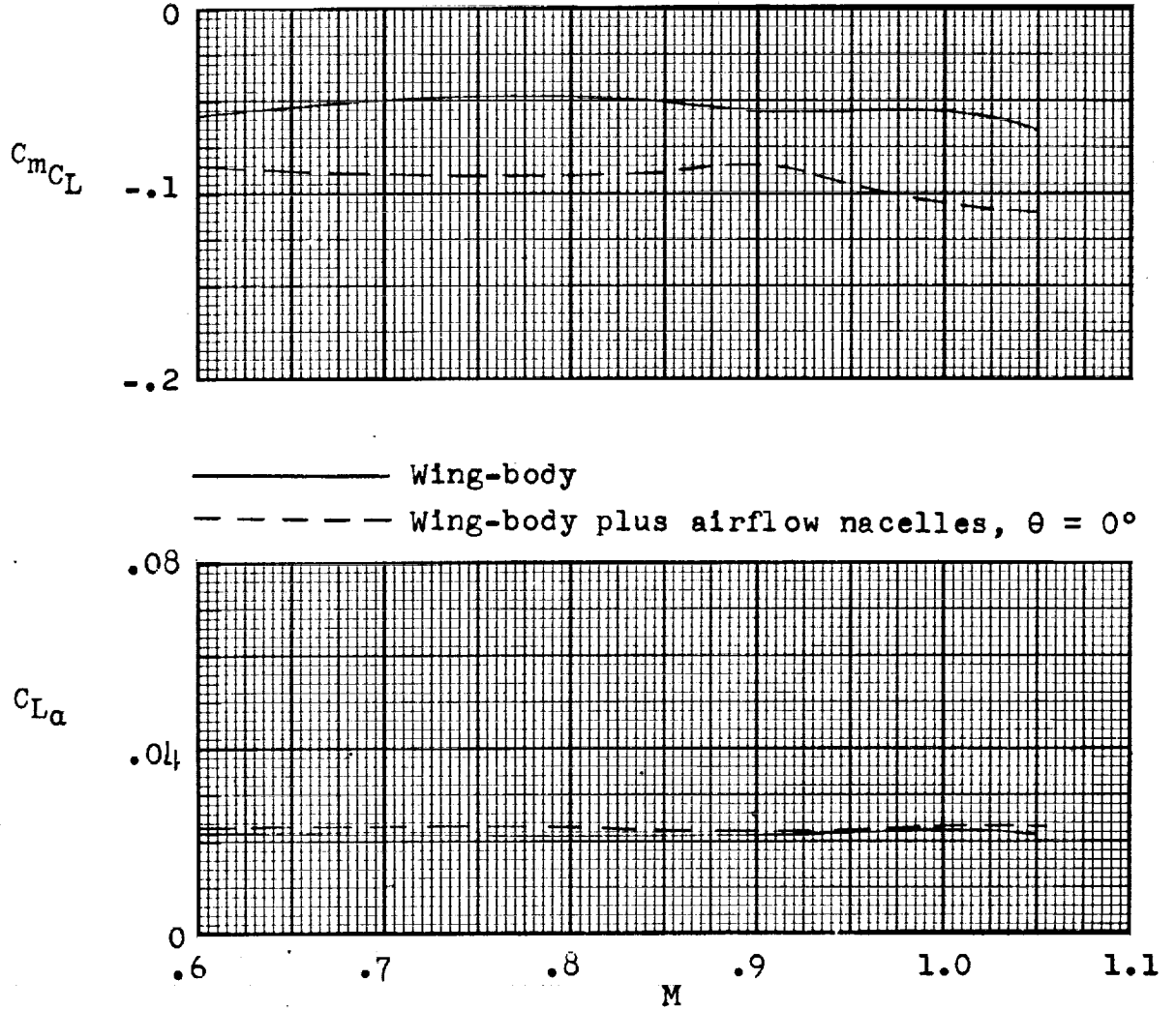


(b) Effect of Mach number on minimum drag coefficient and lift-drag characteristics.

Figure 8.- Continued.

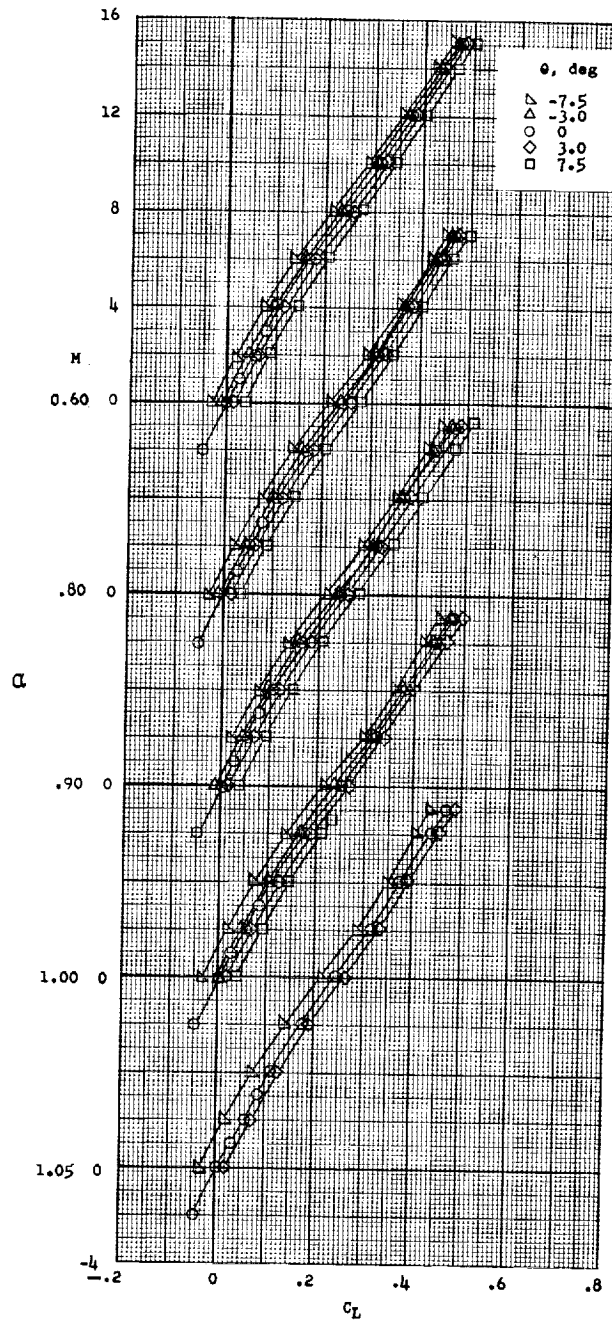


SECRET



(c) Variation of C_{mC_L} and $C_{L\alpha}$ with M .

Figure 8.- Concluded.

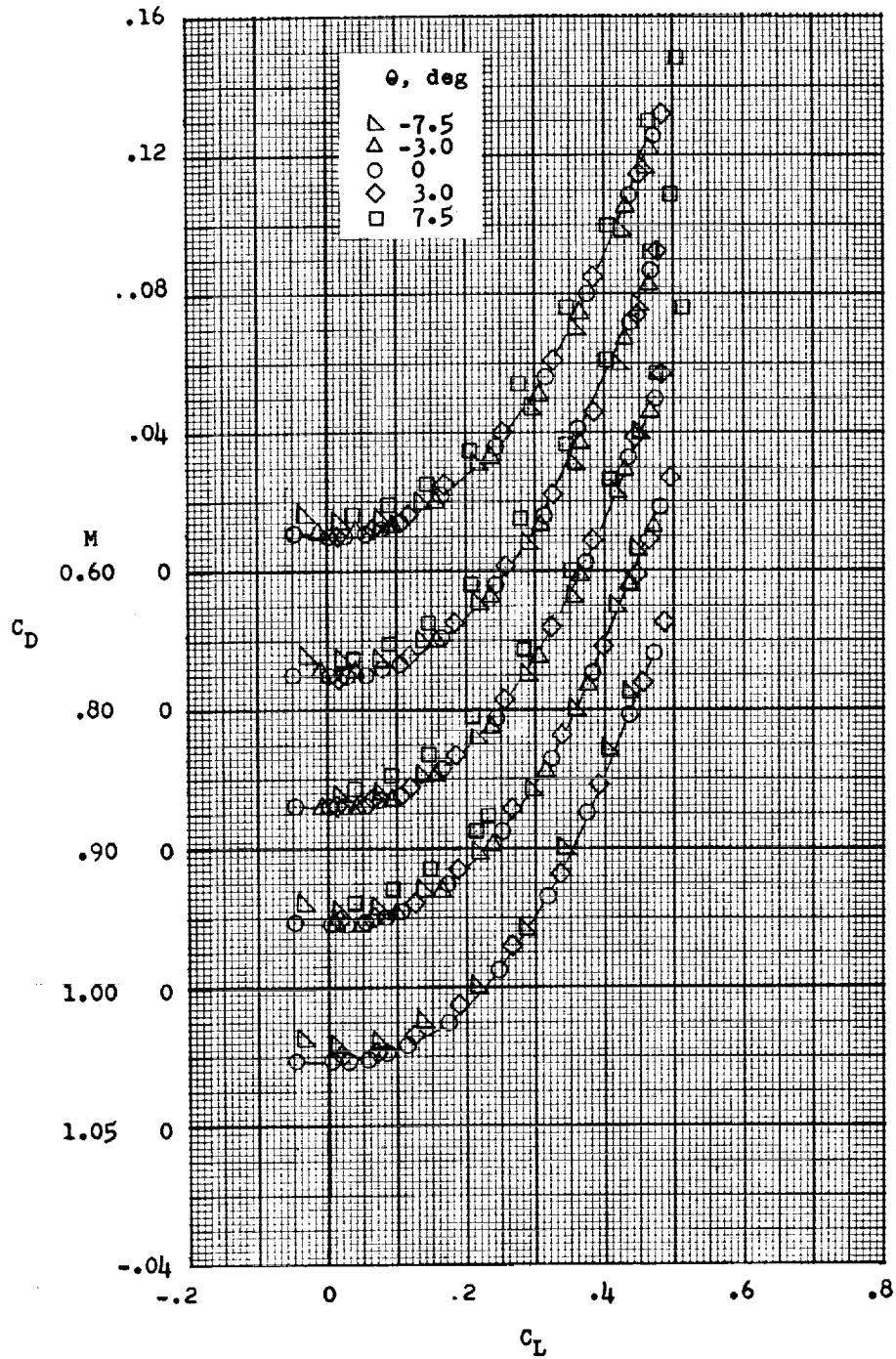


(a) Effect of nacelle pitch deflection on lift coefficient.

Figure 9.- Longitudinal control characteristics. Airflow nacelles with fins; $\Lambda = 75^\circ$; $\delta = 0^\circ$; $\beta = 0^\circ$.

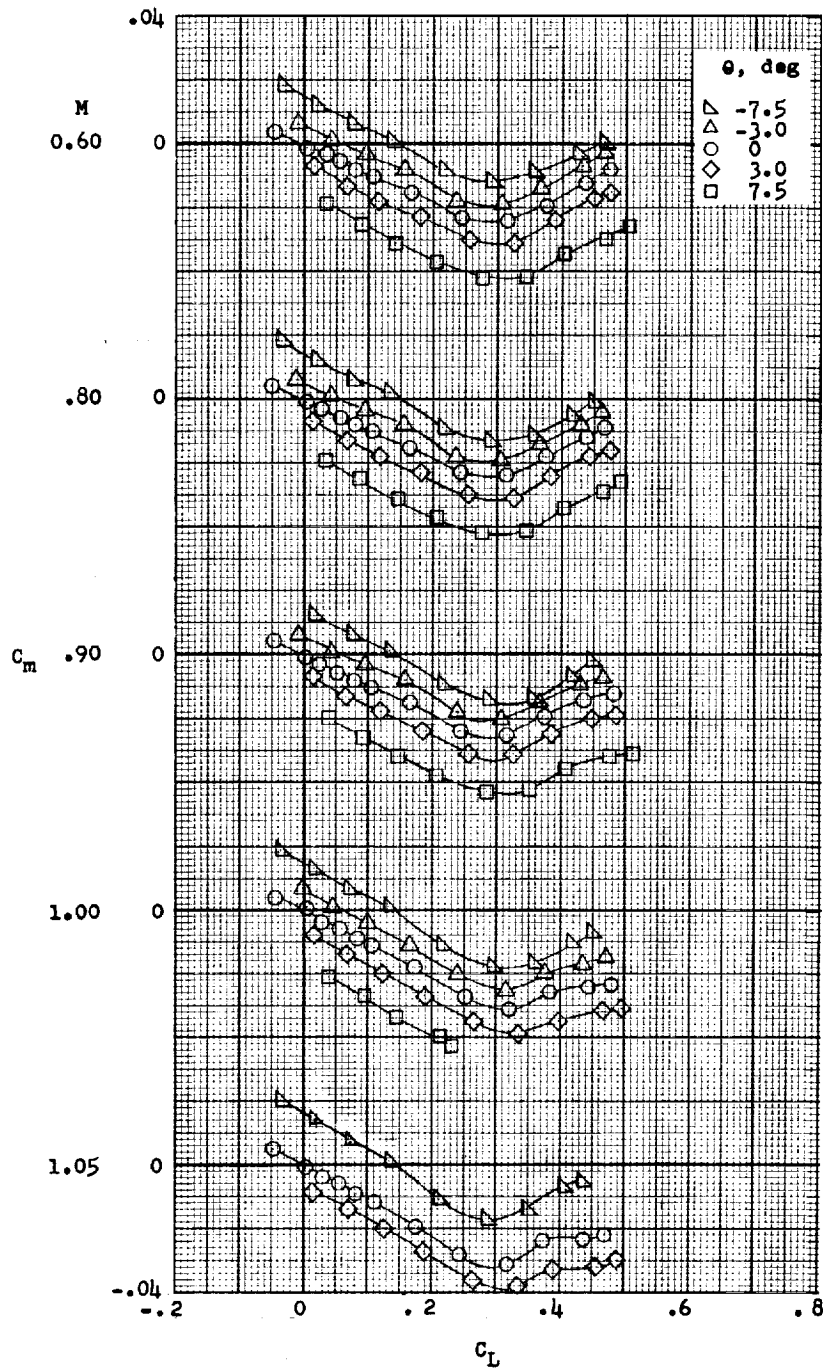


SECRET



(b) Effect of nacelle pitch deflection on drag coefficient.

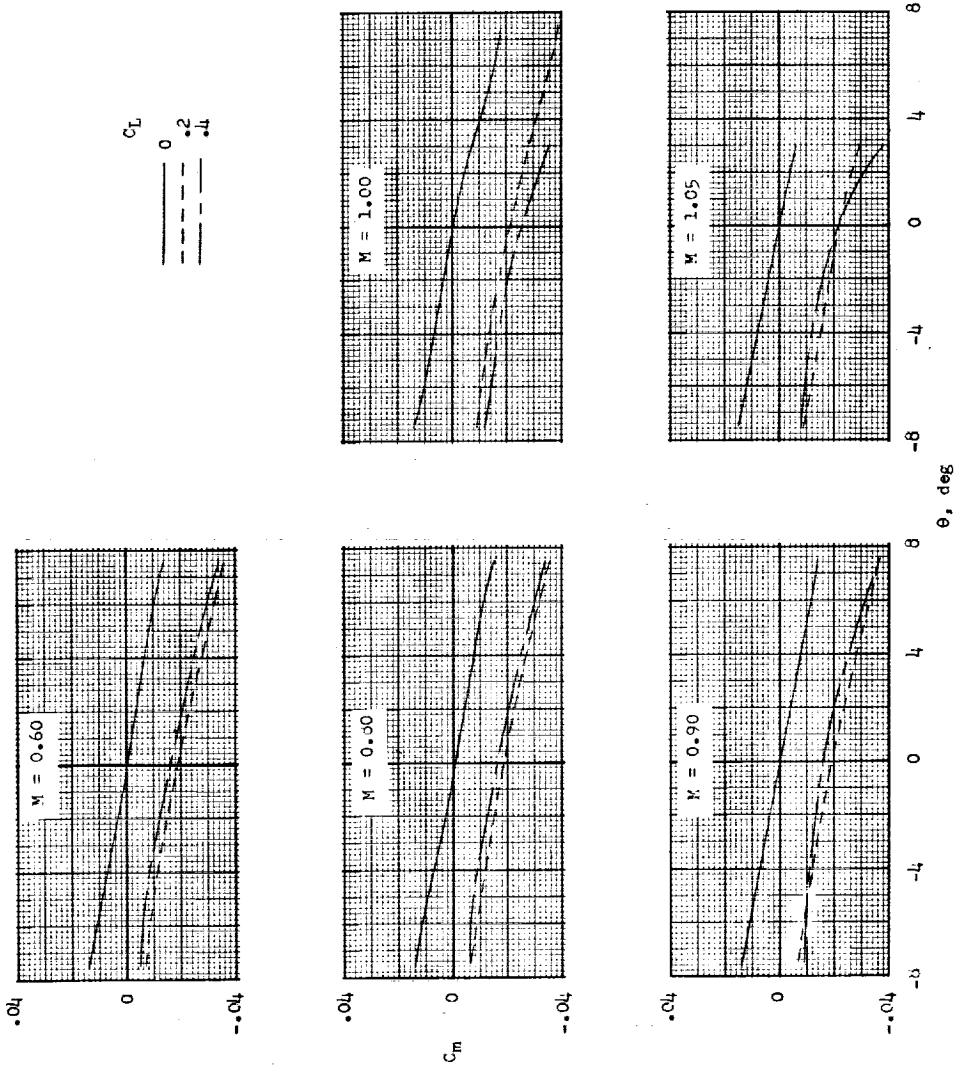
Figure 9.- Continued.



(c) Effect of nacelle pitch deflection on pitching-moment coefficient.

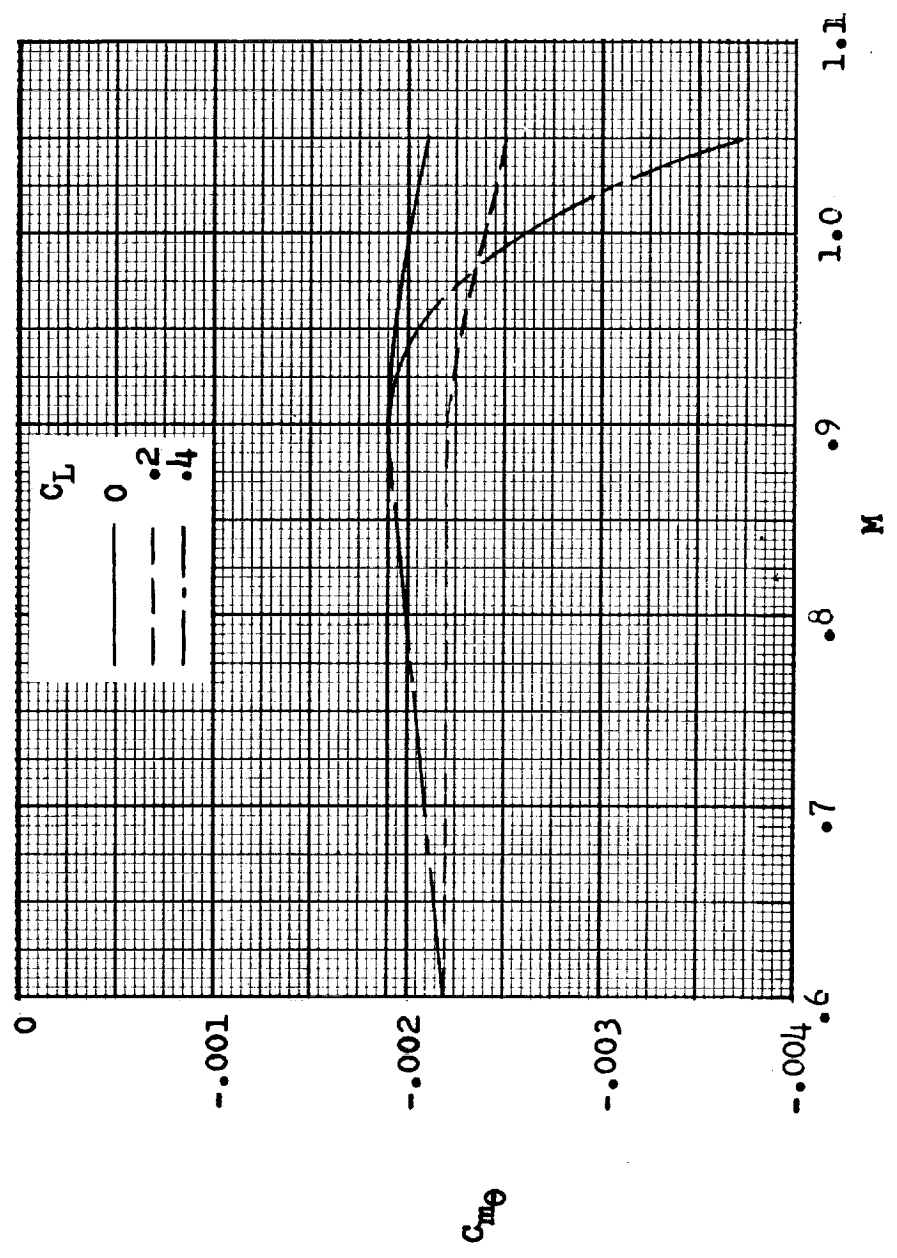
Figure 9.- Concluded.





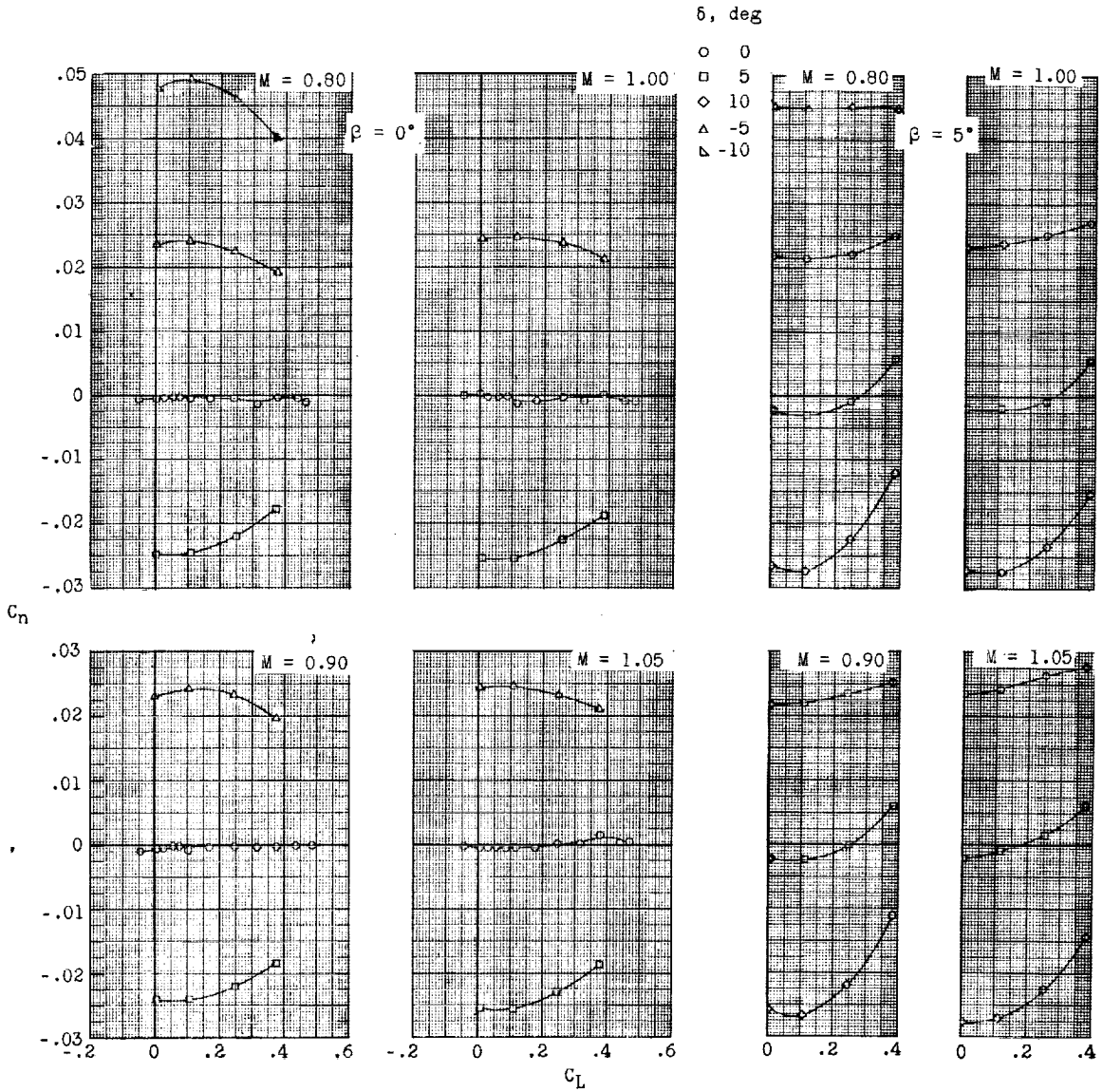
(a) Variation of C_m with θ .

Figure 10.- Longitudinal control effectiveness. Airflow nacelles with fins; $\Lambda = 75^\circ$; $\delta = 0^\circ$; $\beta = 0^\circ$.



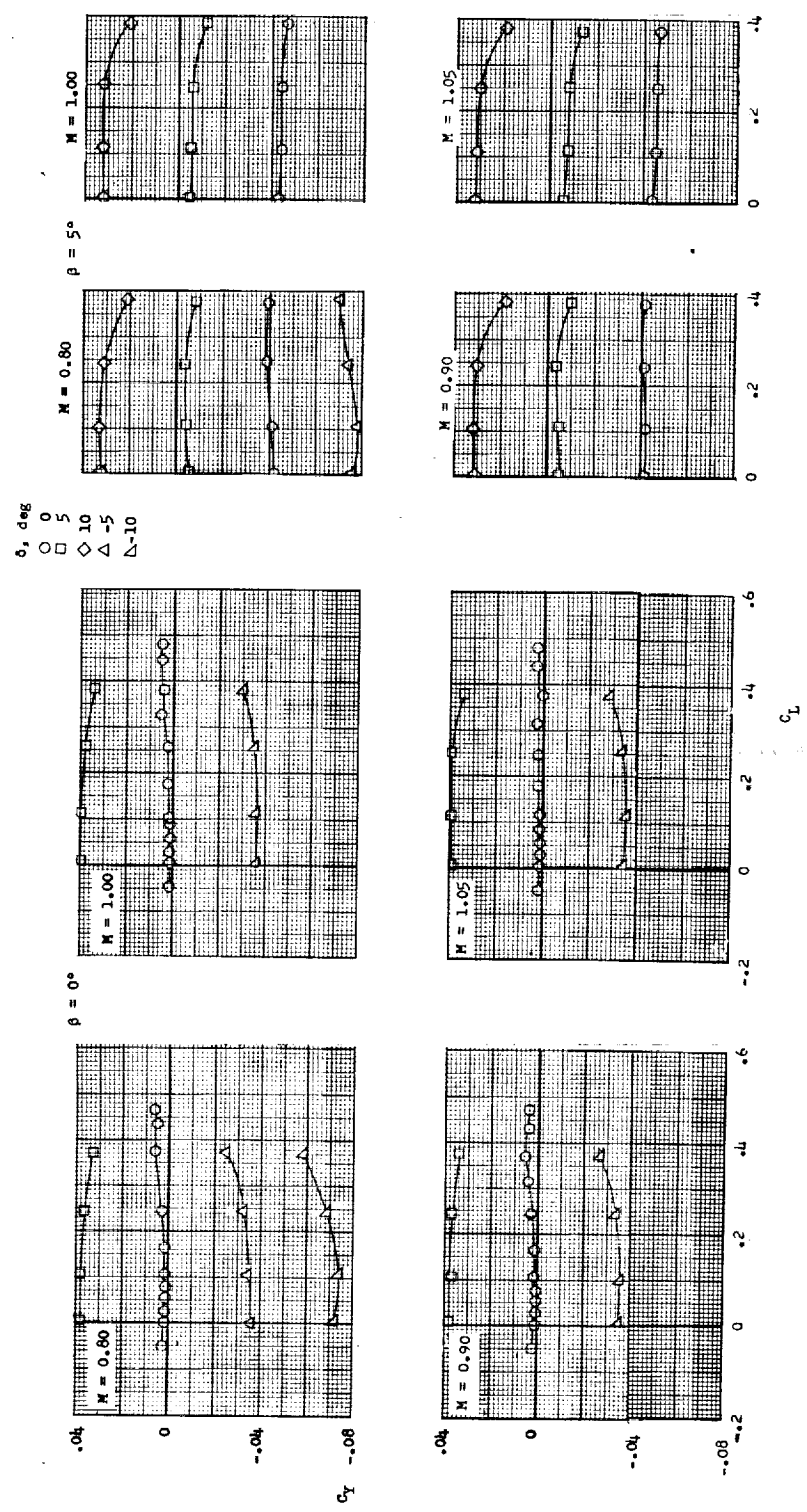
(b) Variation of $C_{m\theta}$ with M .

Figure 10.- Concluded.



(a) Effect of nacelle yaw deflection on yawing-moment coefficient.

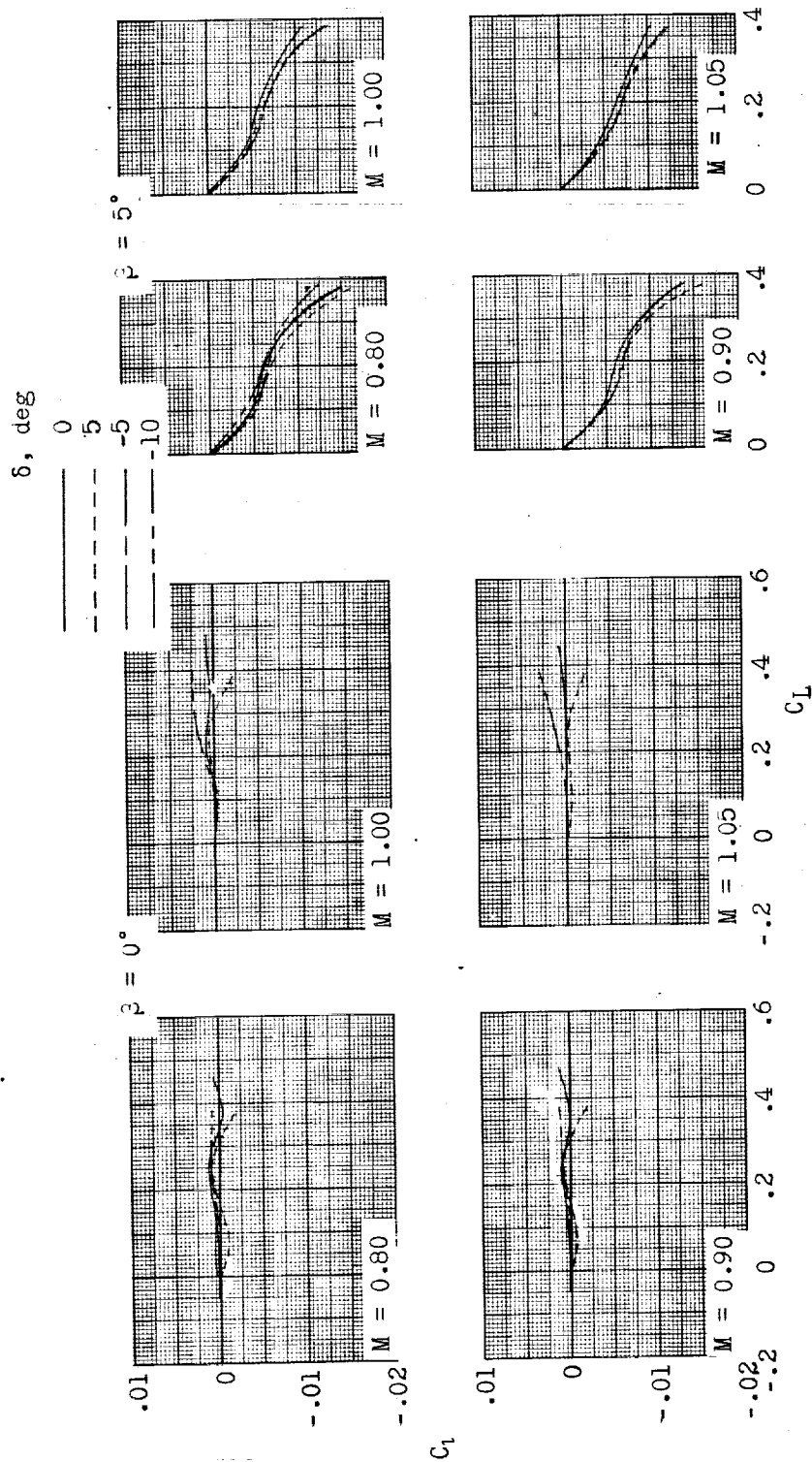
Figure 11.- Directional control characteristics. Airflow nacelles with fins; $\Lambda = 75^\circ$; $\theta = 0^\circ$; $\beta = 0^\circ$ and 5° .



(b) Effect of nacelle yaw deflection on side-force coefficient.

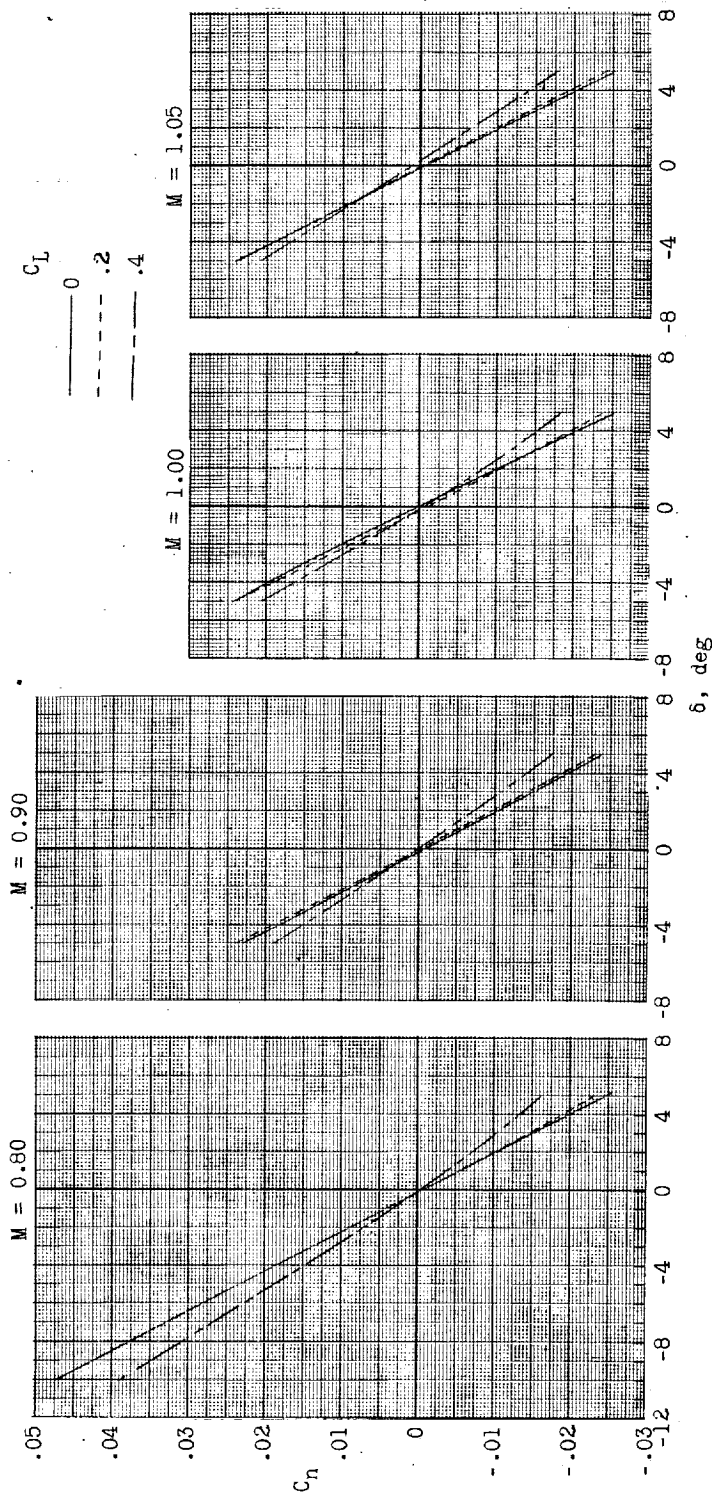
Figure 11.- Continued.

SECRET



(c) Effect of nacelle yaw deflection on rolling-moment coefficient.

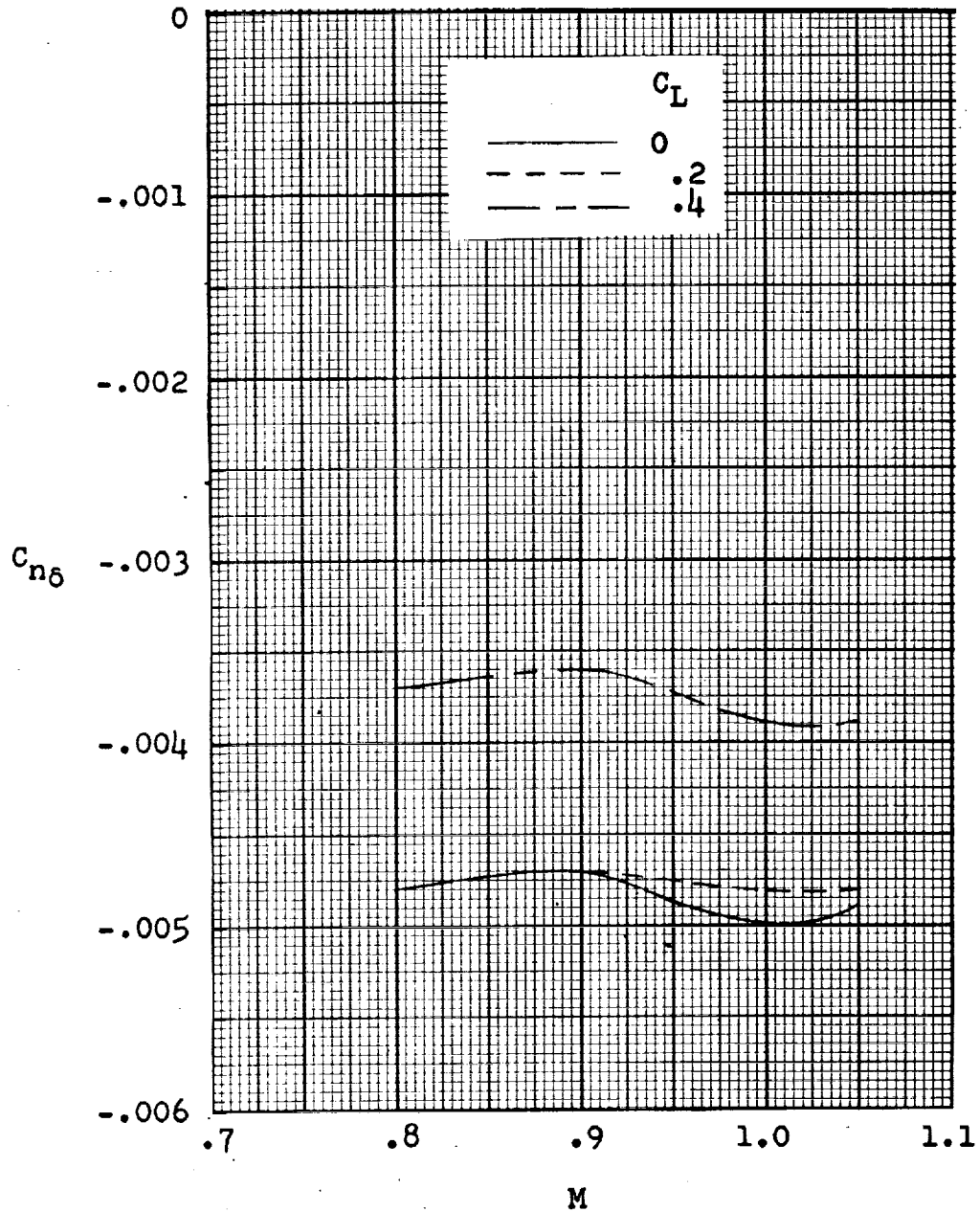
Figure 11.- Concluded.



(a) Variation of C_n with δ .

Figure 12.- Directional control effectiveness. Airflow nacelles with fins; $\Lambda = 75^\circ$; $\theta = 0^\circ$; $\beta = 0^\circ$.

SECRET



(b) Variation of $C_{n\delta}$ with M .

Figure 12.- Concluded.

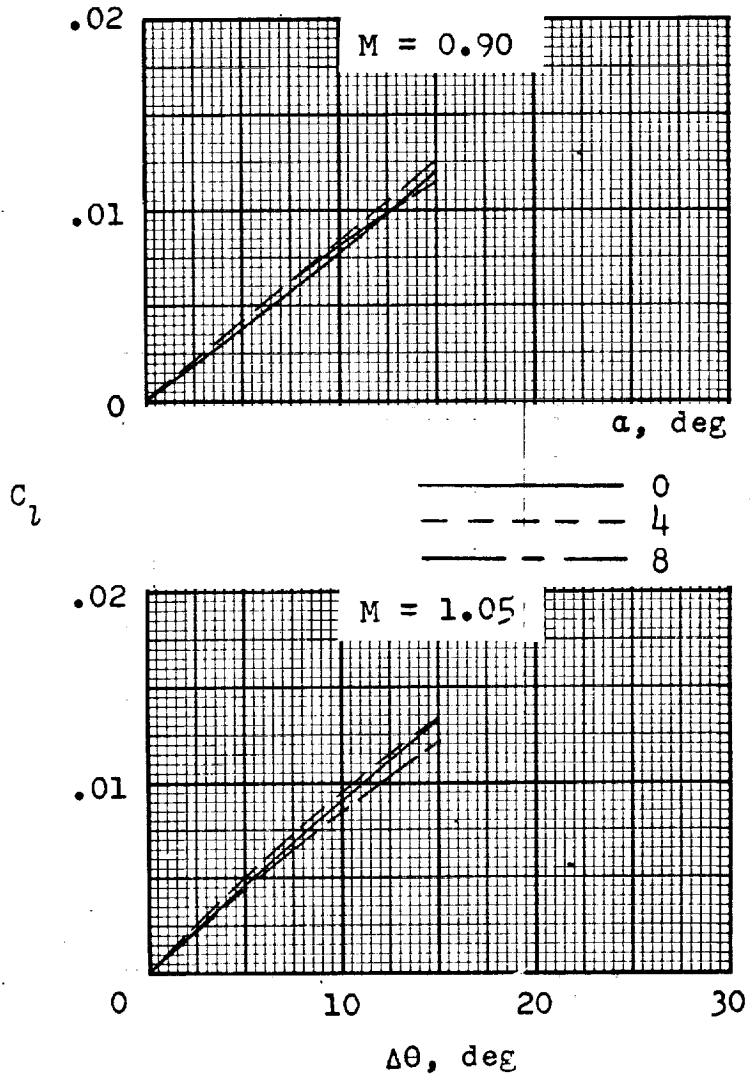
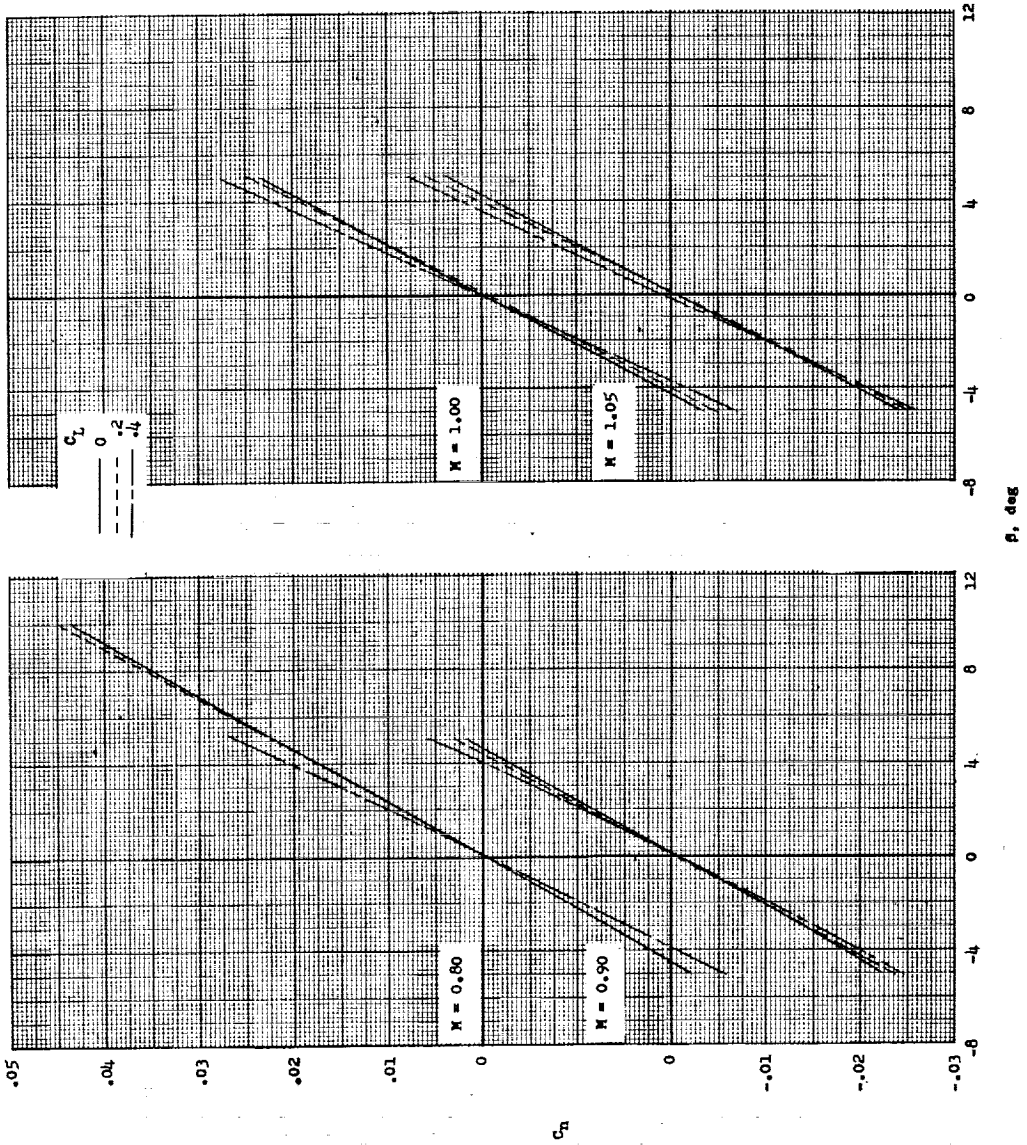


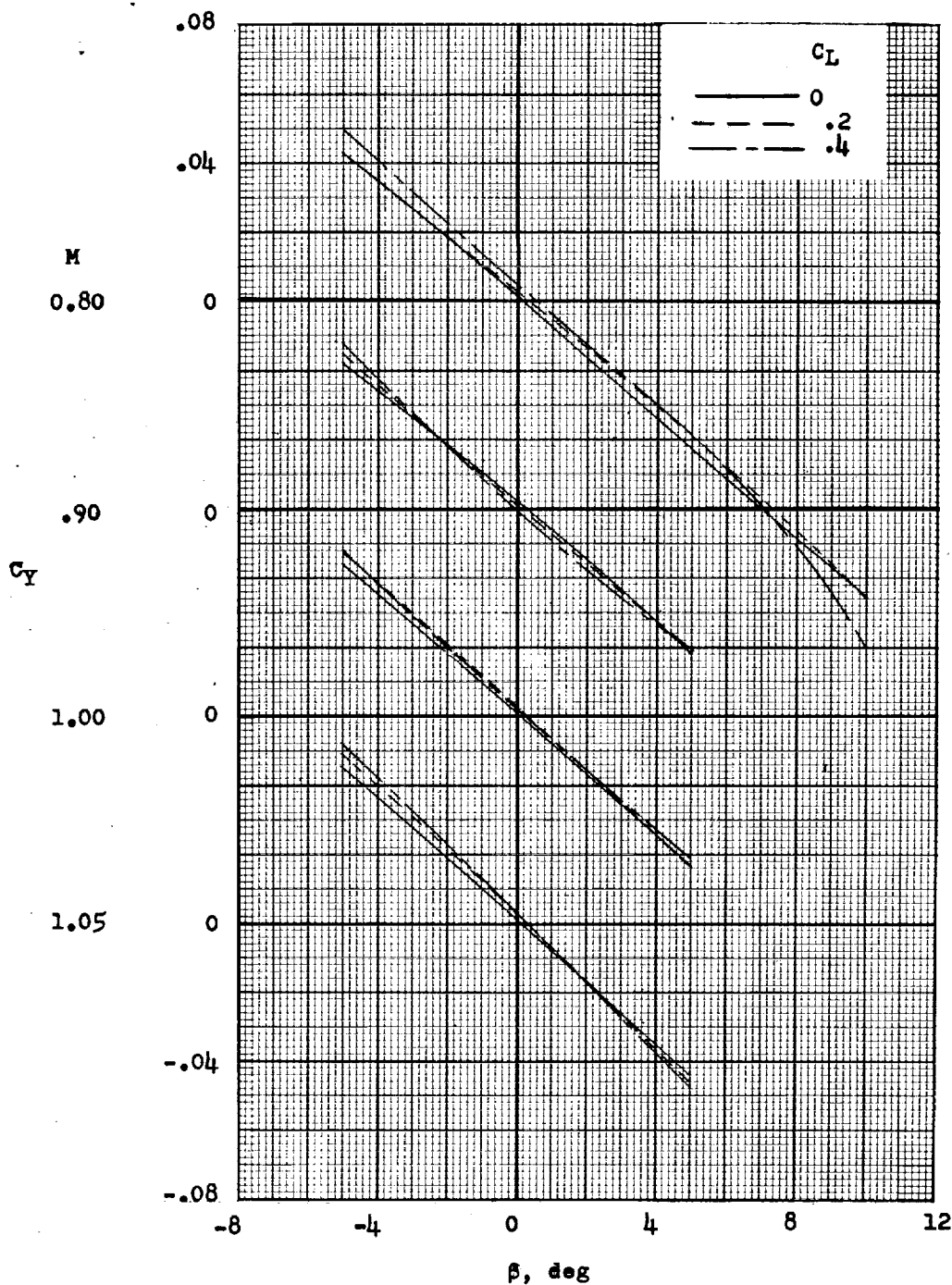
Figure 13.- Lateral control effectiveness. Jet nacelles; $\Lambda = 75^\circ$; $\delta = 0^\circ$; $\beta = 0^\circ$.





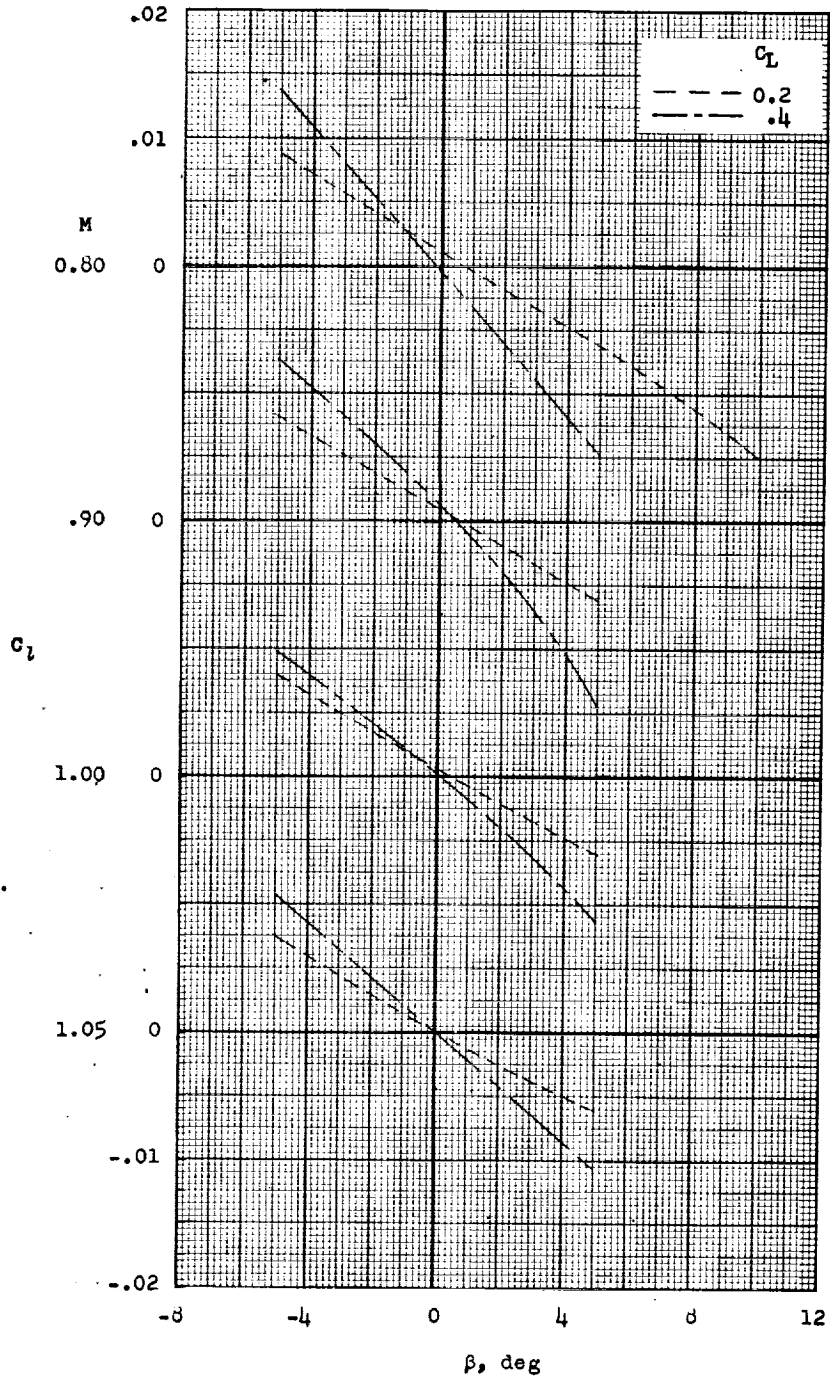
(a) Variation of C_n with β .

Figure 14.- Directional and lateral stability characteristics. $A = 75^\circ$; $\theta = 0^\circ$; $\delta = 0^\circ$.



(b) Variation of C_Y with β .

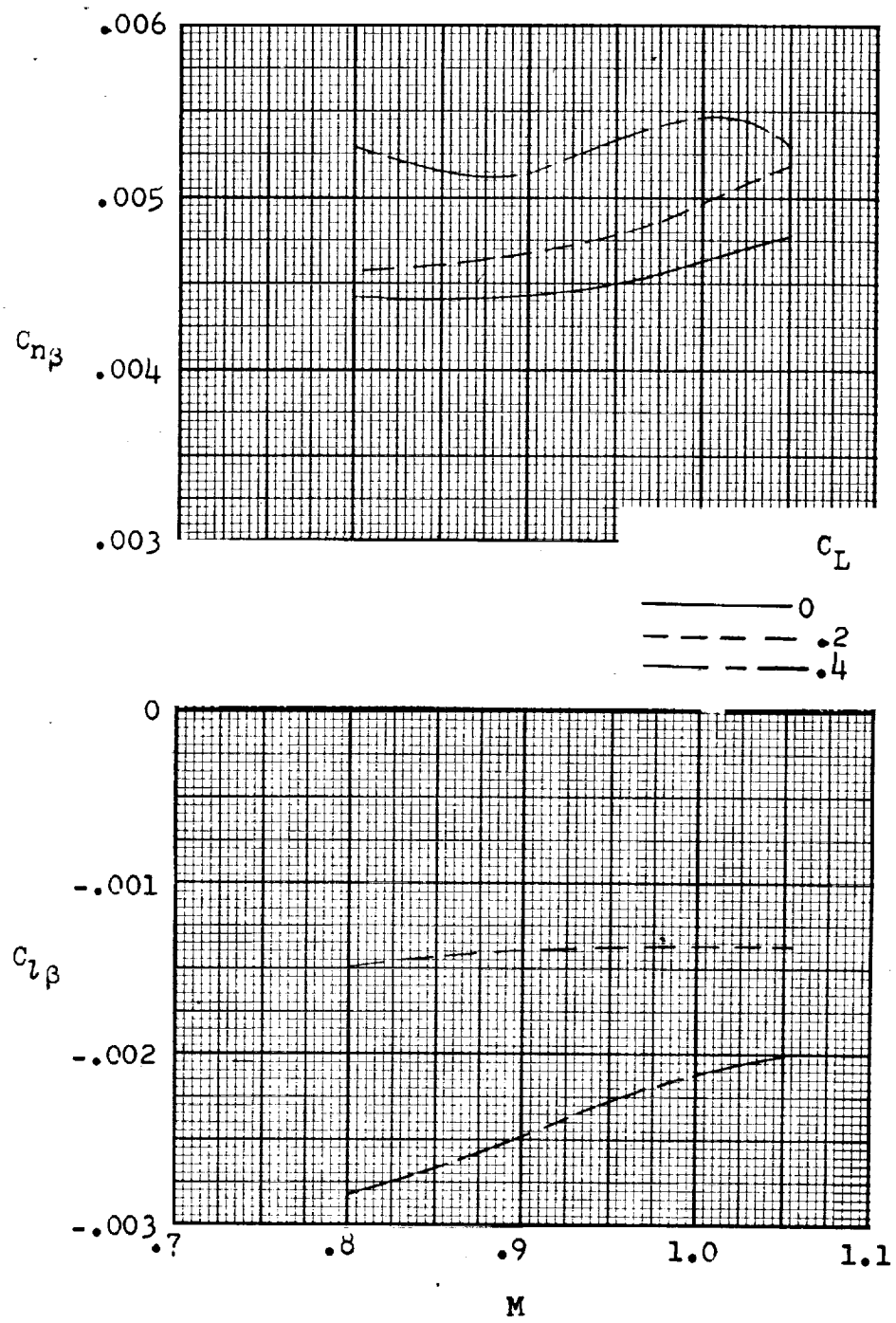
Figure 14.- Continued.



(c) Variation of C_2 with β .

Figure 14.- Continued.

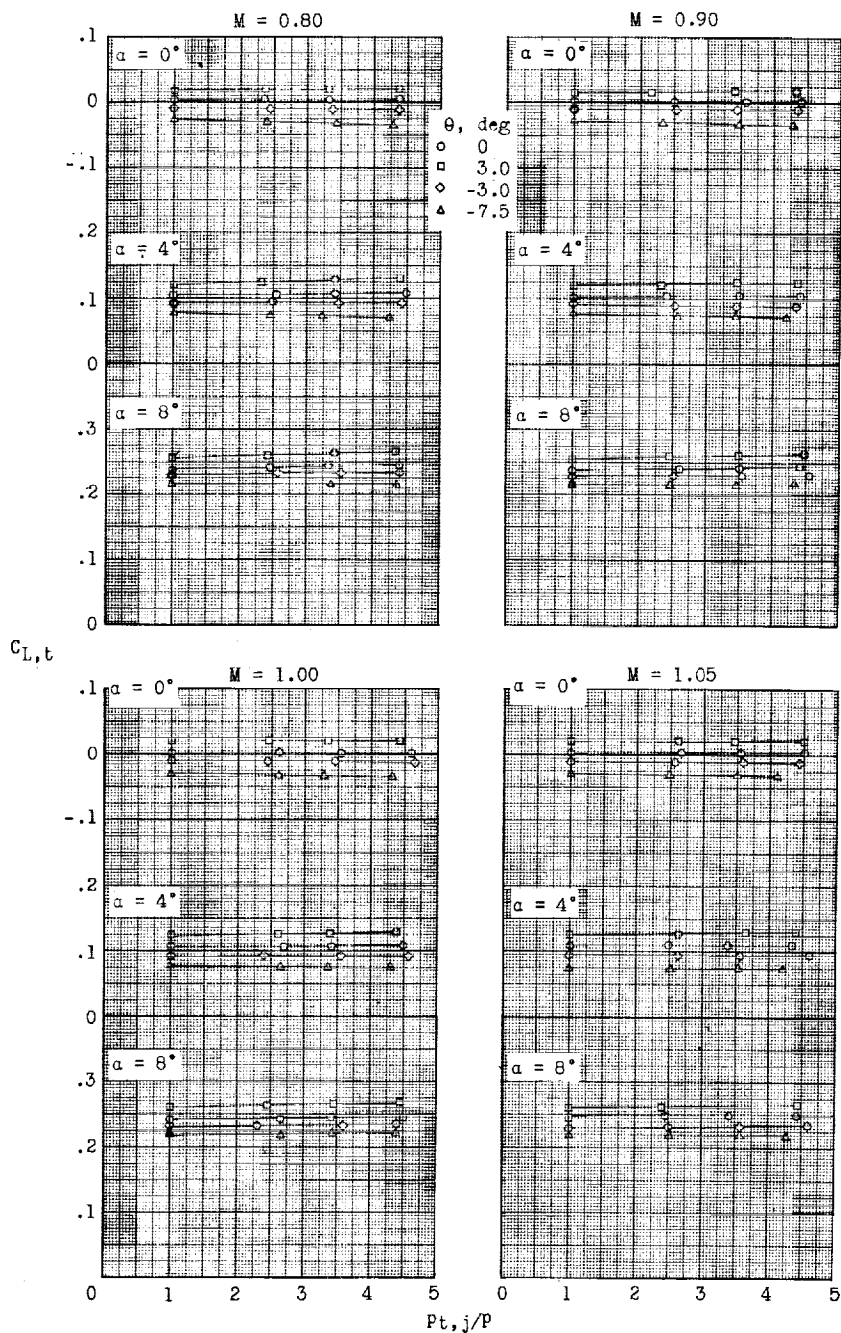
~~SECRET~~



(d) Variation of $C_{n\beta}$ and $C_{l\beta}$ with M .

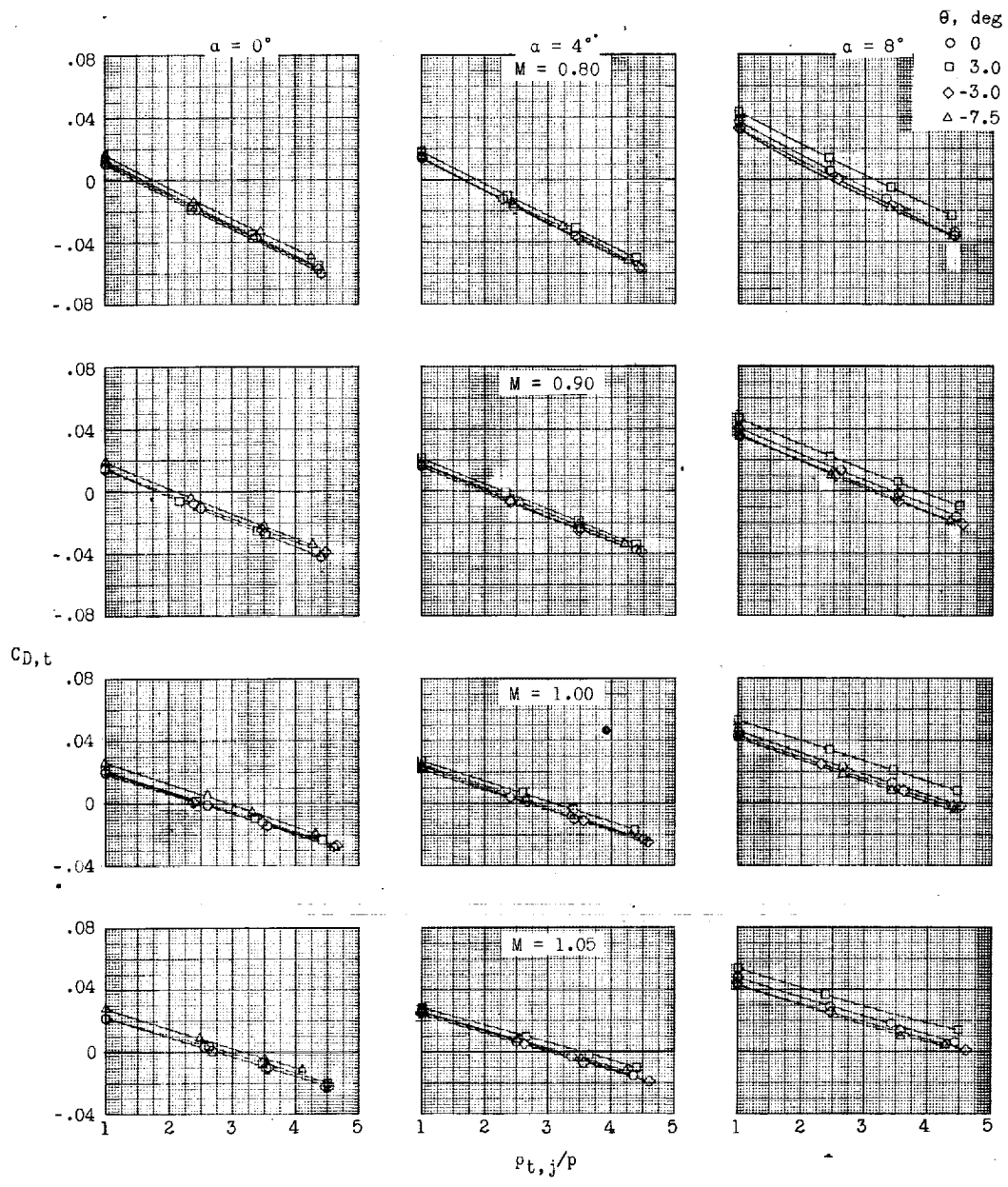
Figure 14.- Concluded.





(a) Variation of lift coefficient with jet total-pressure ratio.

Figure 15.- Model forces and moments (including components of jet thrust) for several nacelle pitch deflections.

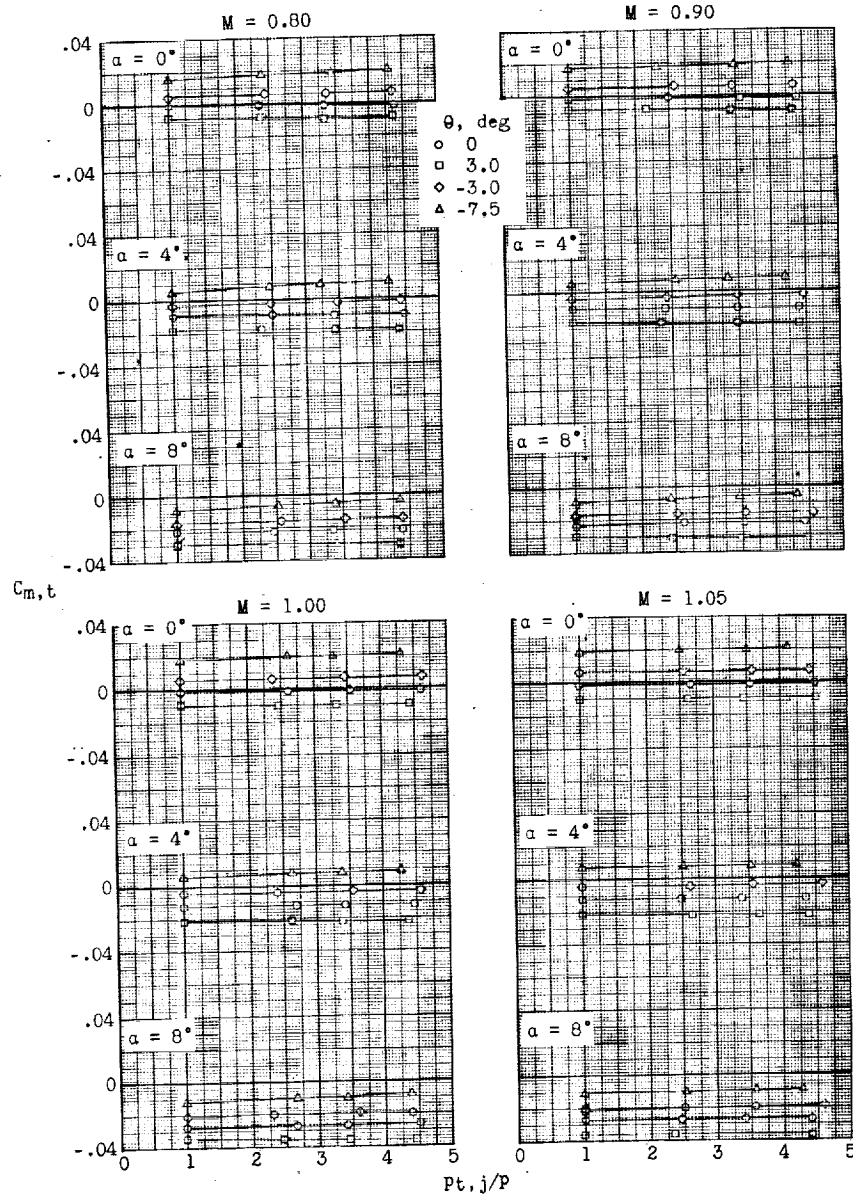


(b) Variation of drag coefficient with jet total-pressure ratio.

Figure 15.- Continued.

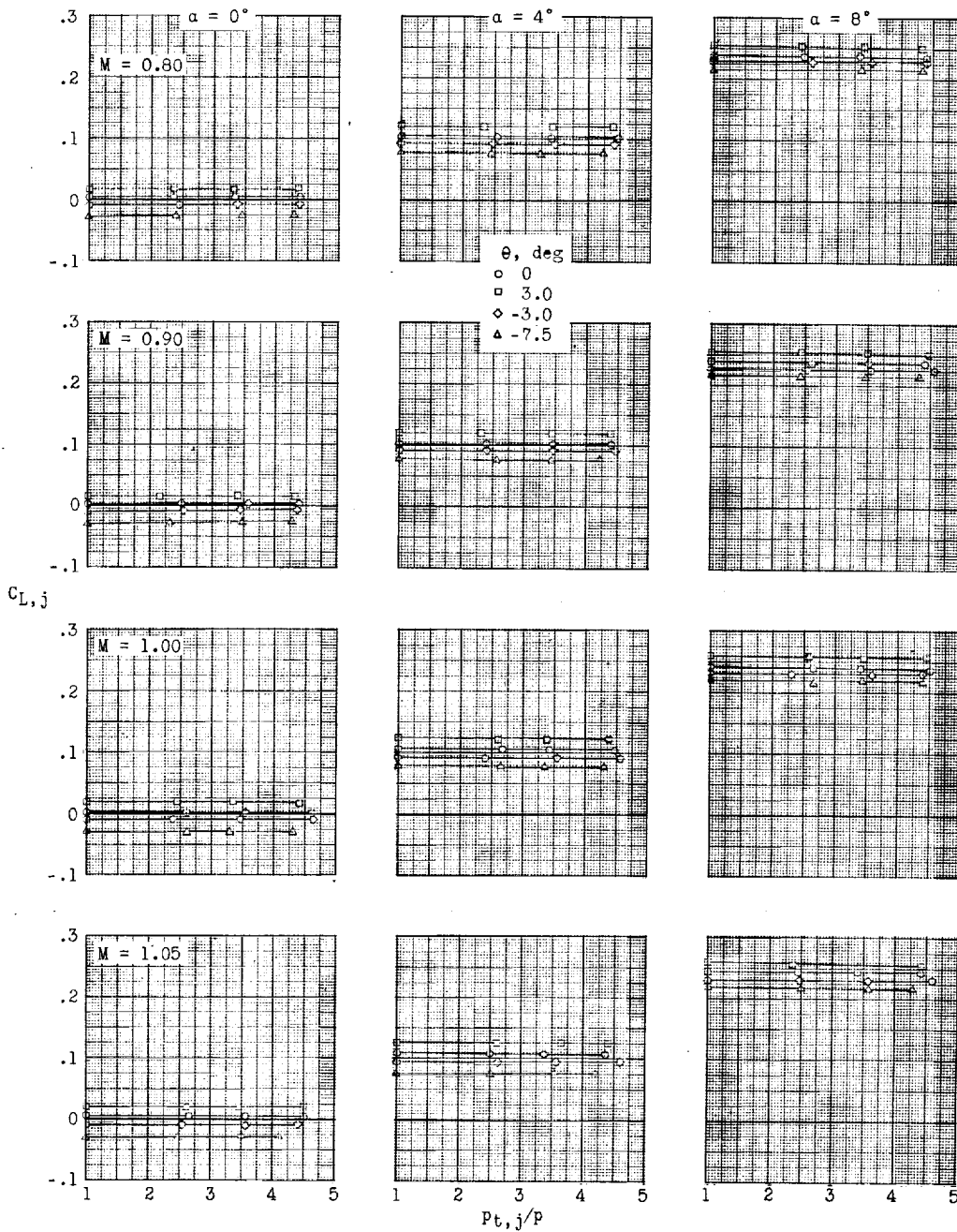


SECRET



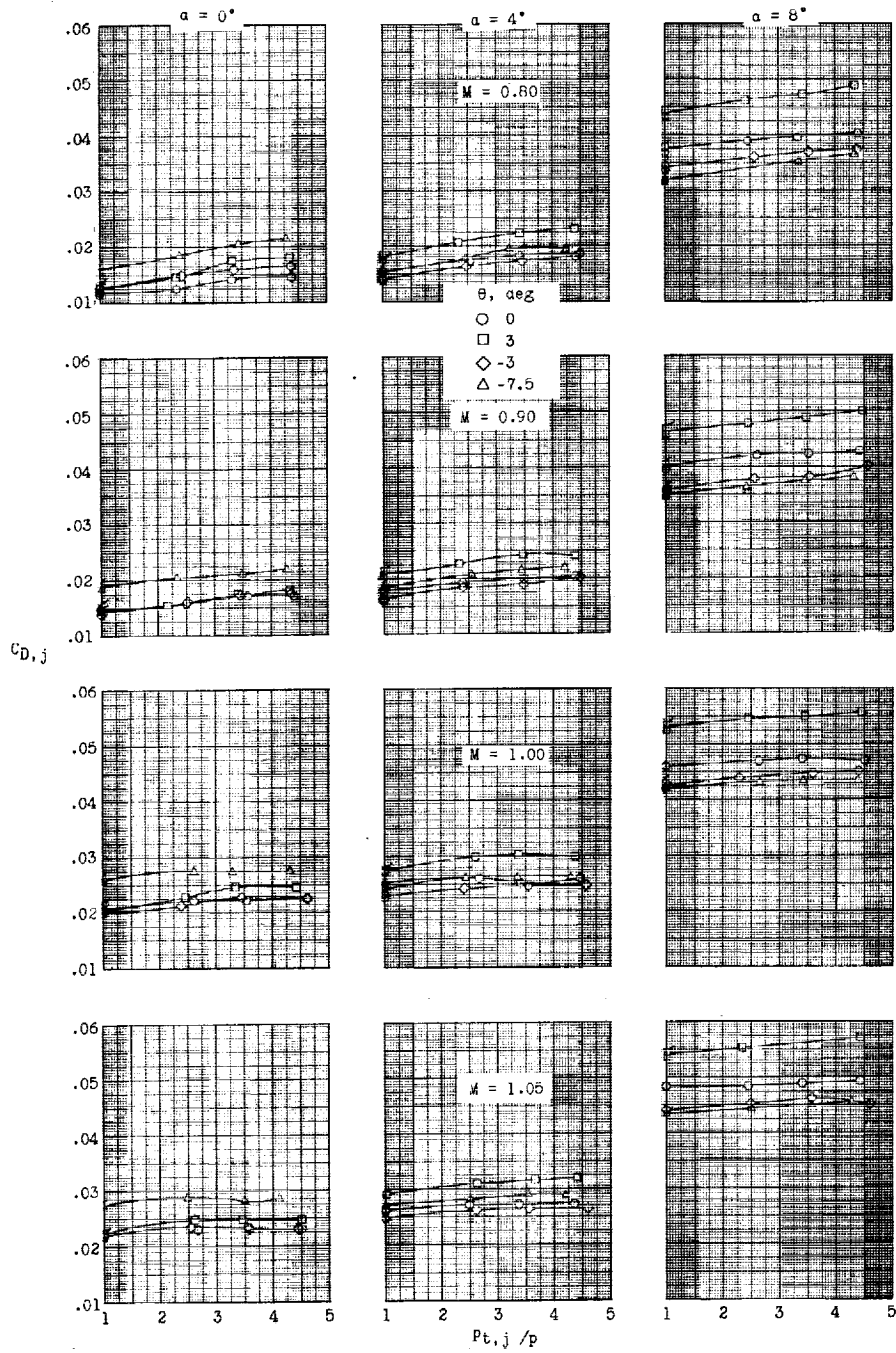
(c) Variation of pitching-moment coefficient with jet total-pressure ratio.

Figure 15.- Concluded.



(a) Variation of lift coefficient with jet total-pressure ratio.

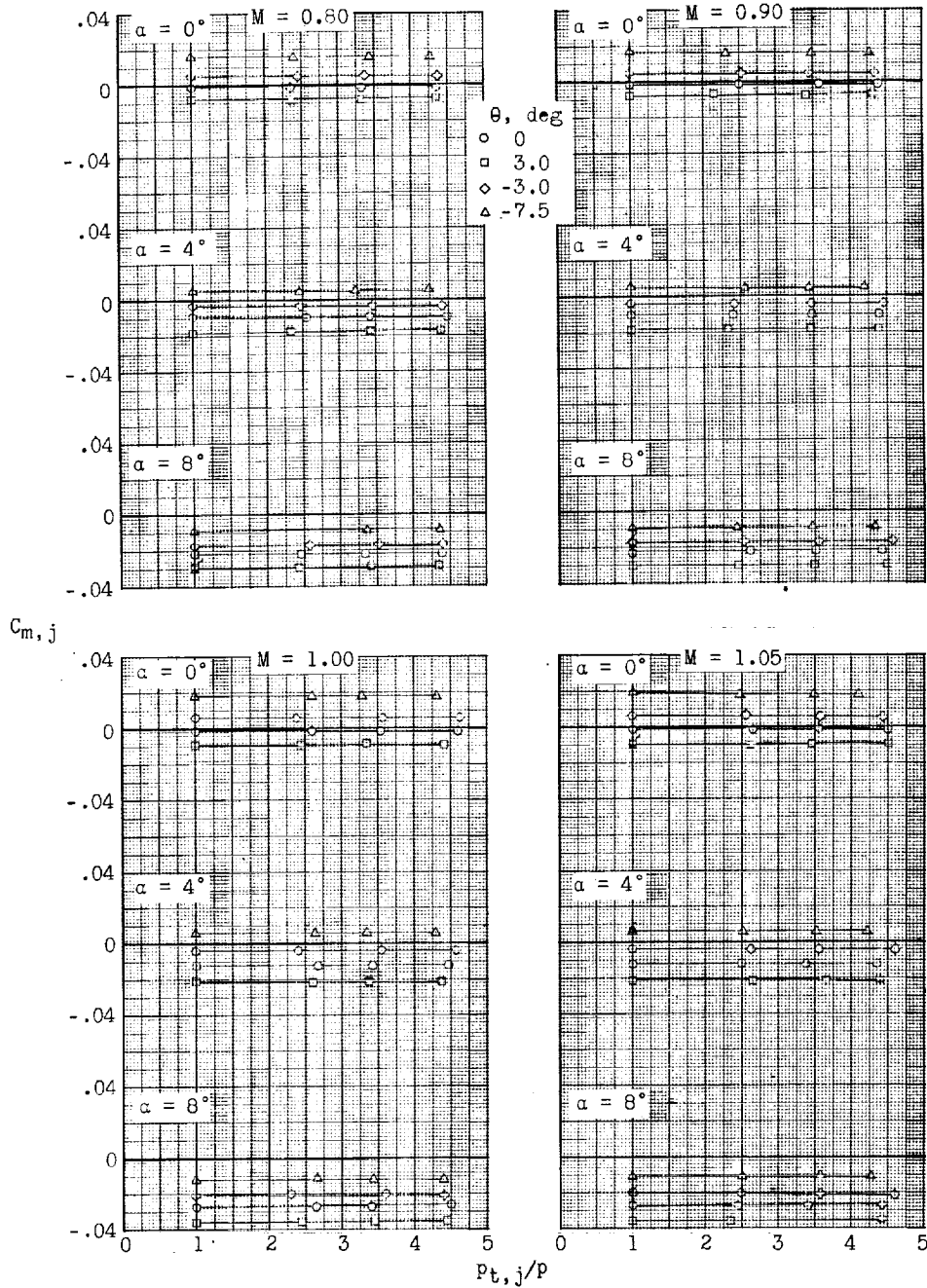
Figure 16.- Model forces and moment (with components of jet thrust removed) for several nacelle pitch deflections.



(b) Variation of drag coefficient with jet total-pressure ratio.

Figure 16.- Continued.

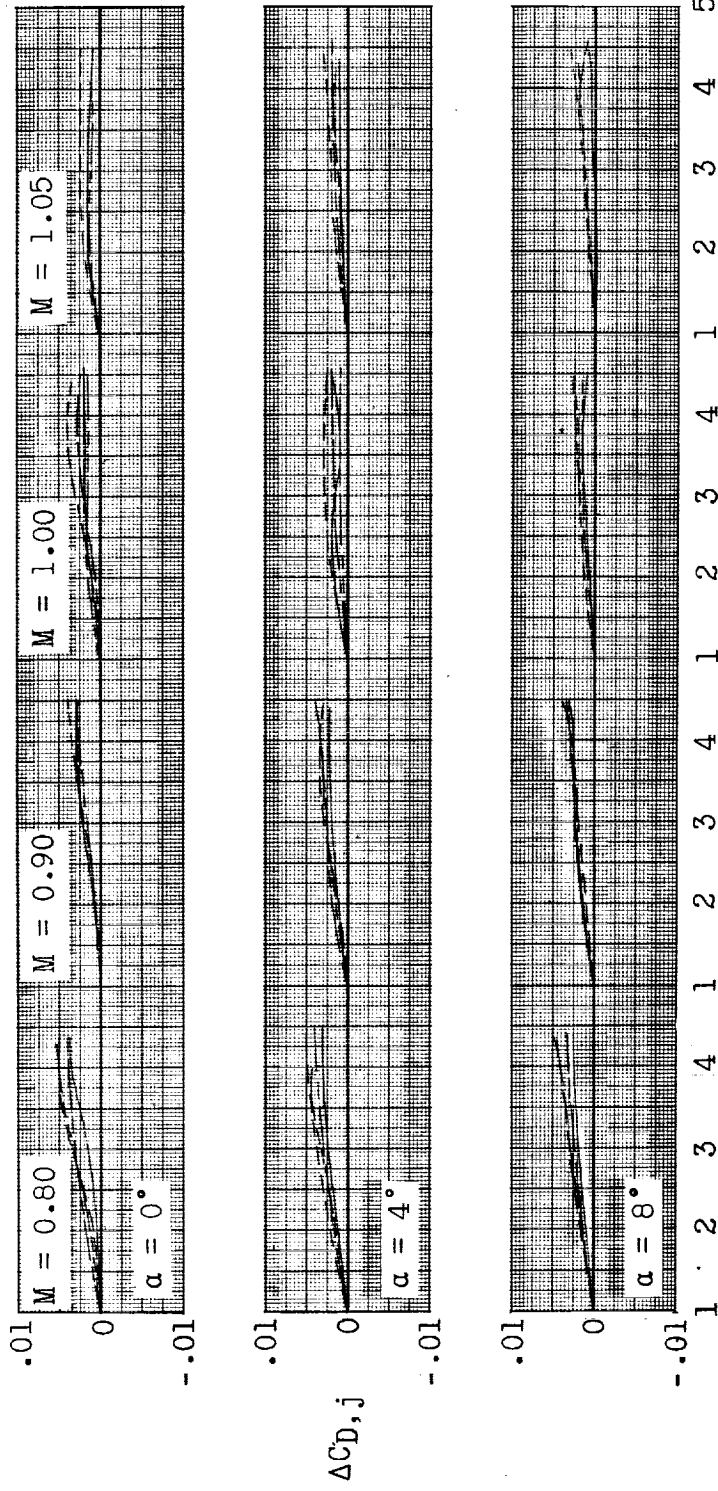
SECRET



(c) Variation of pitching-moment coefficient with jet total-pressure ratio.

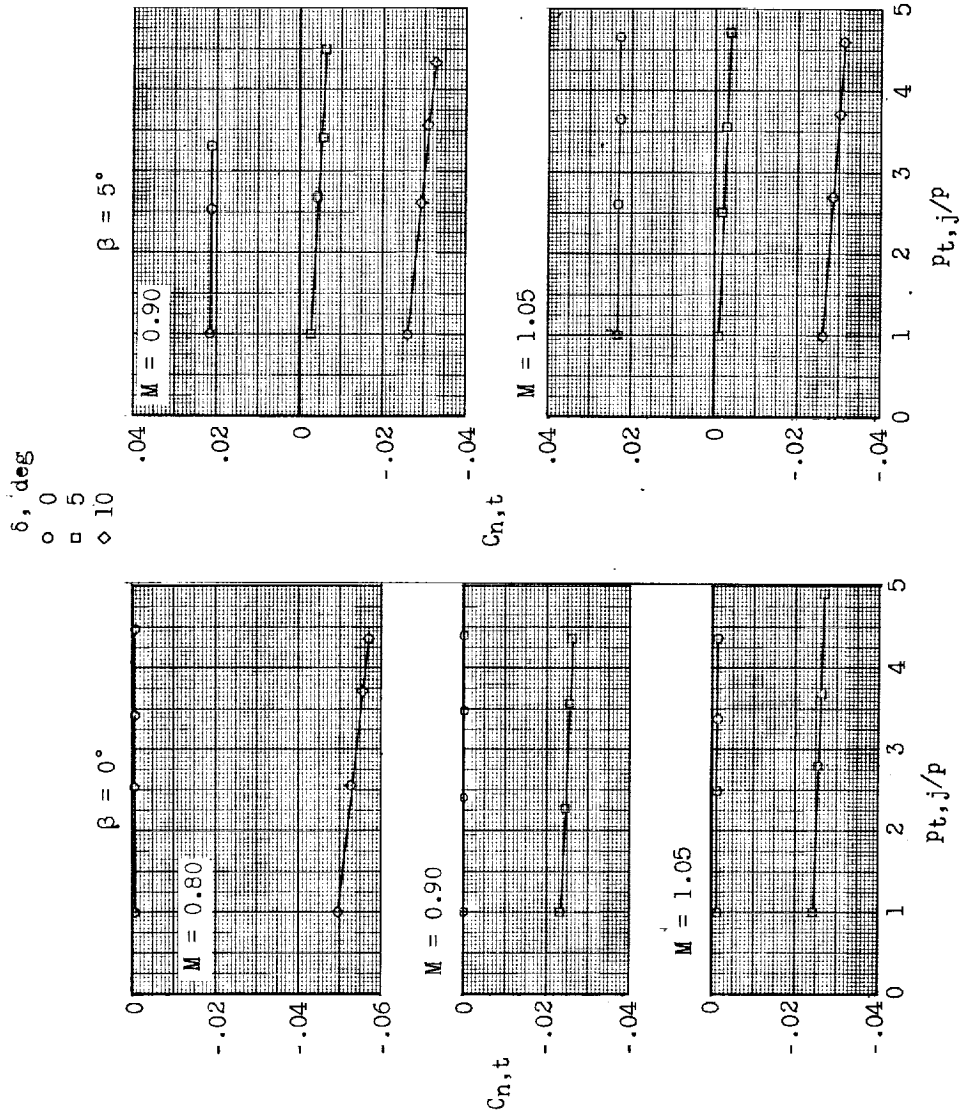
Figure 16.- Concluded.

θ , deg
 ——— 0
 - - - 3.0
 - - - -3.0
 - - - -7.5



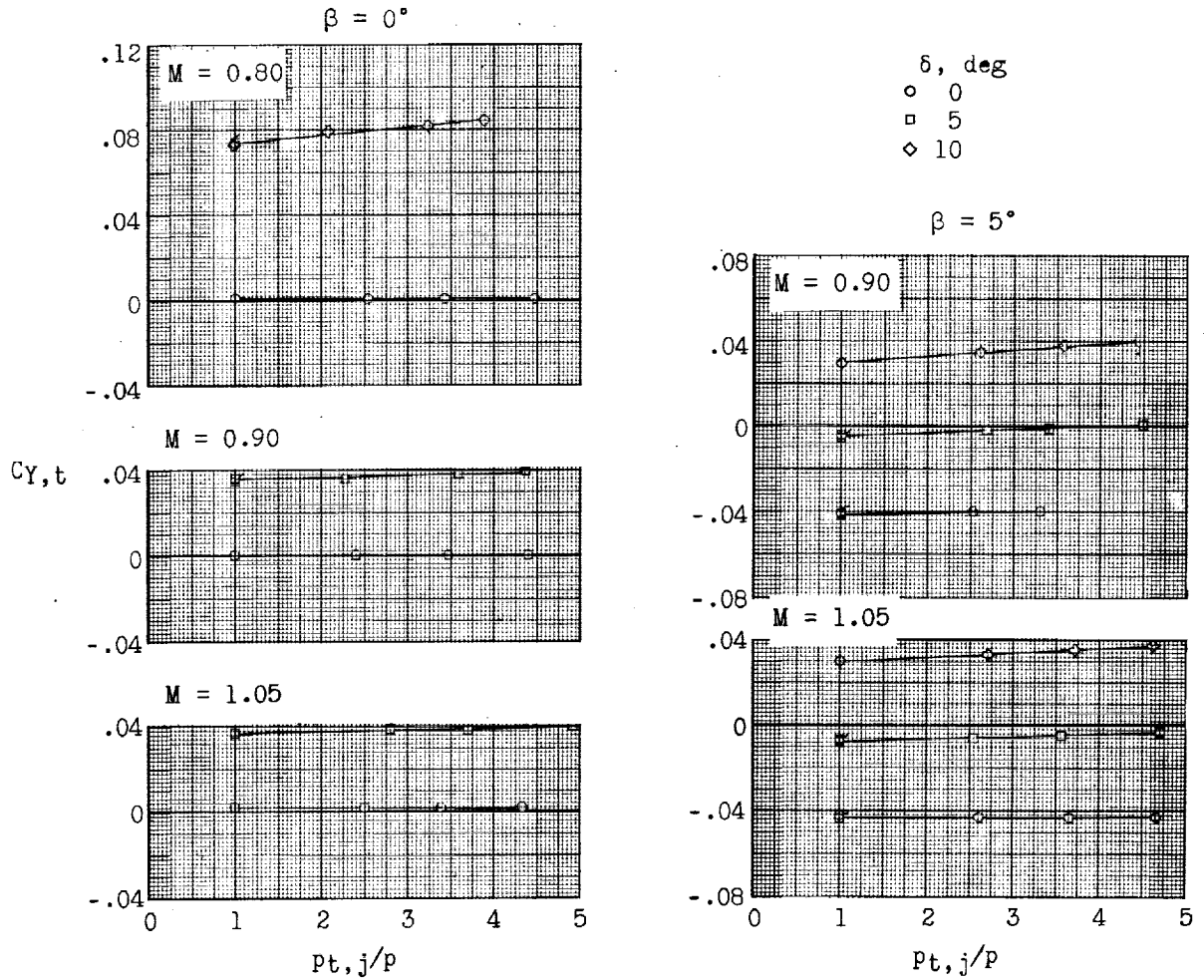
$P_{t,j}/P$

Figure 17.- Variation of incremental drag coefficient with jet total-pressure ratio for several nacelle pitch angles.



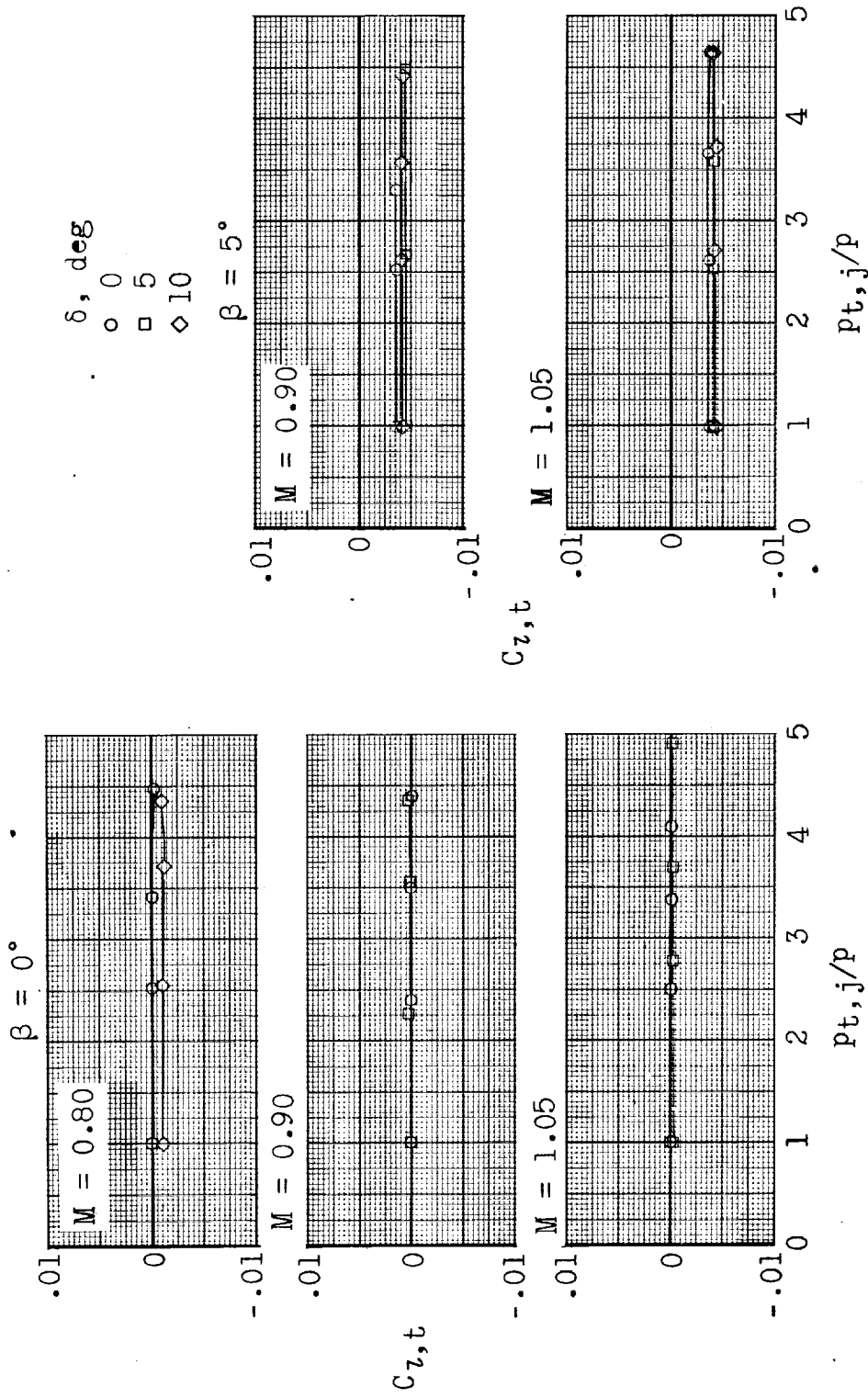
(a) Variation of yawing-moment coefficient with jet total-pressure ratio.

Figure 18.- Lateral forces and moments (including components of jet thrust) for several nacelle lateral deflections. $\beta = 0^\circ$ and 5° ; $\alpha = 4^\circ$.



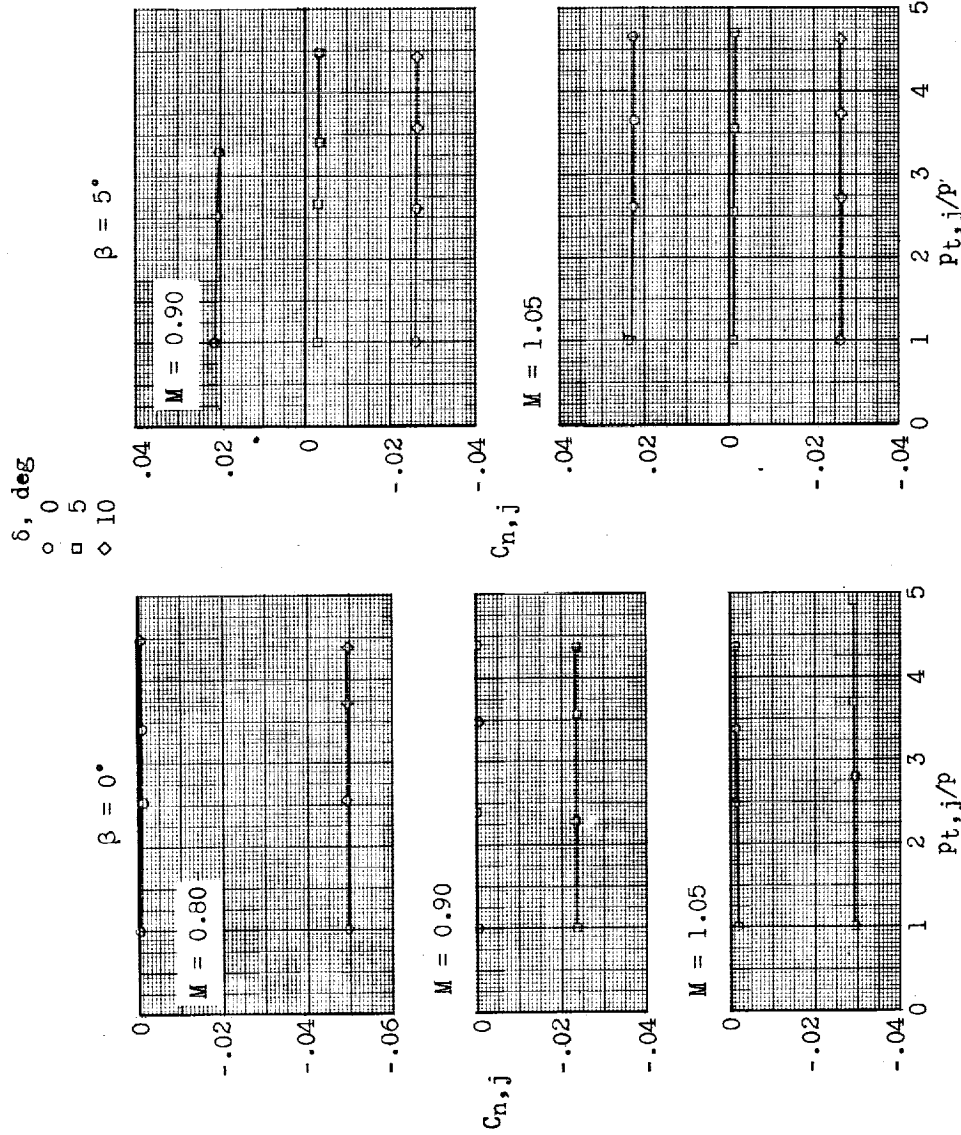
(b) Variation of side-force coefficient with jet total-pressure ratio.

Figure 18.- Continued.



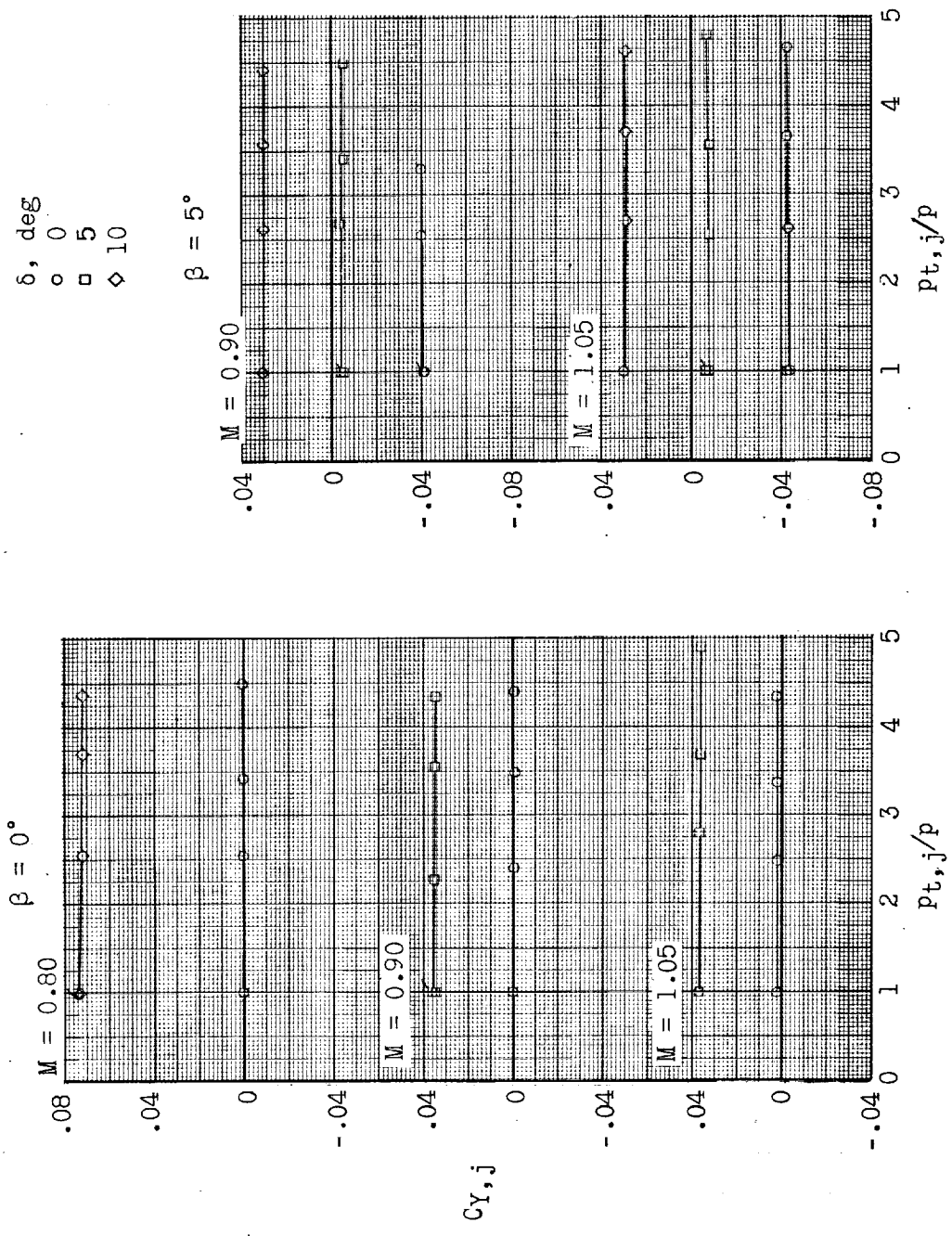
(c) Variation of rolling-moment coefficient with jet total-pressure ratio.

Figure 18.- Concluded.



(a) Variation of yawing-moment coefficient with jet total-pressure ratio.

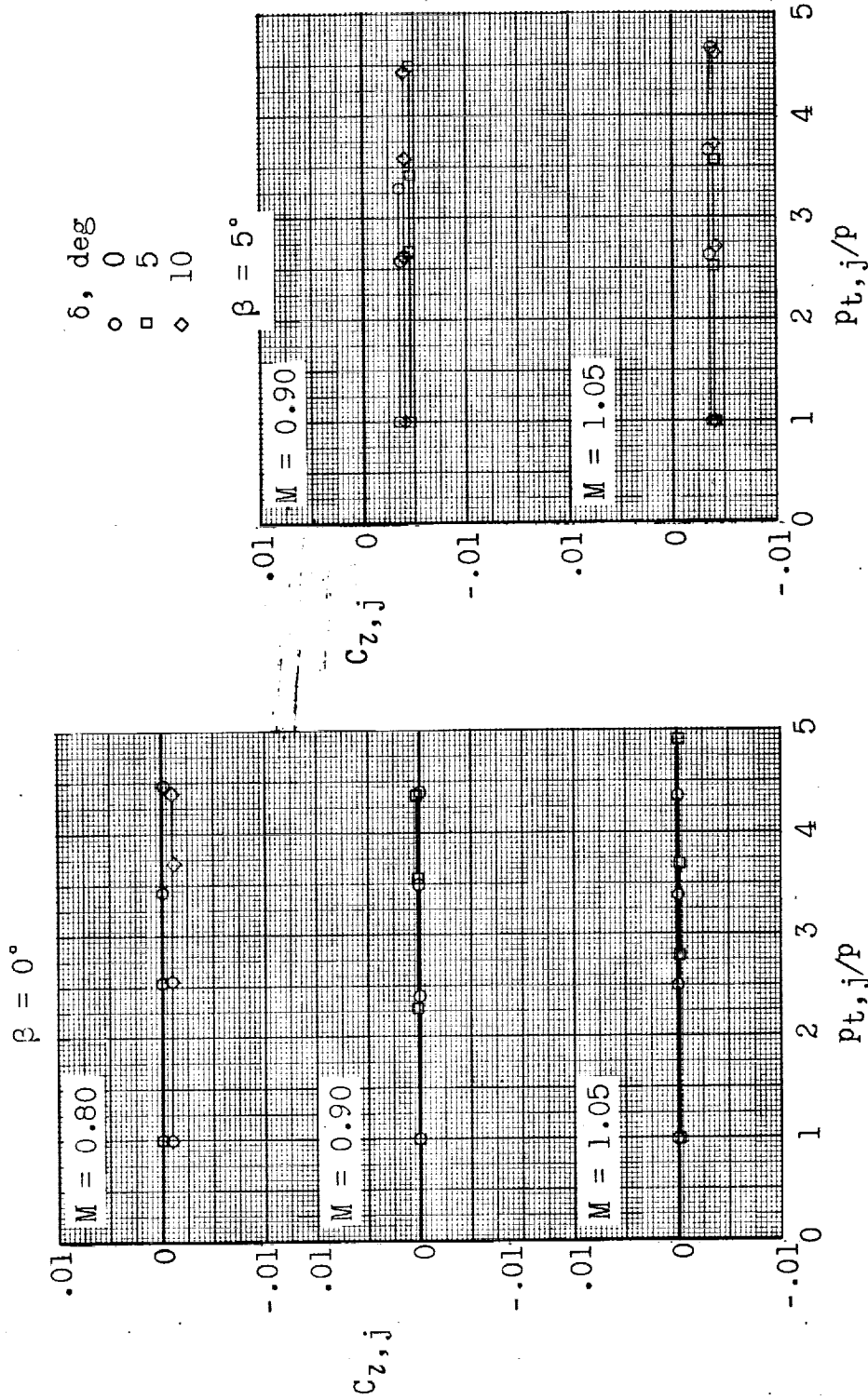
Figure 19.- Lateral forces and moments (with components of jet thrust removed) for several nacelle lateral deflections. $\beta = 0^\circ$ and 5° ; $\alpha = 4^\circ$.



(b) Variation of side-force coefficient with jet total-pressure ratio.

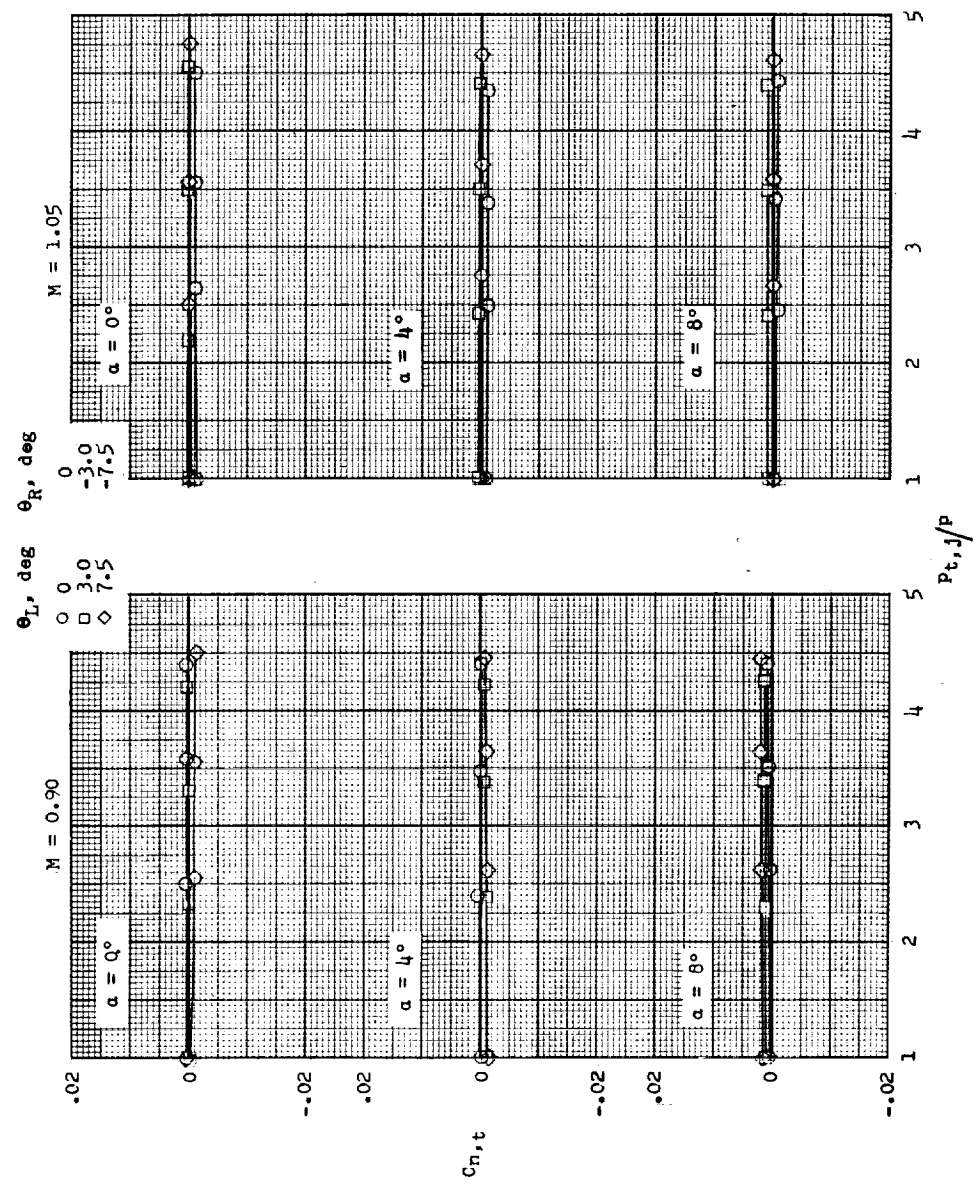
Figure 19.- Continued.

SECRET



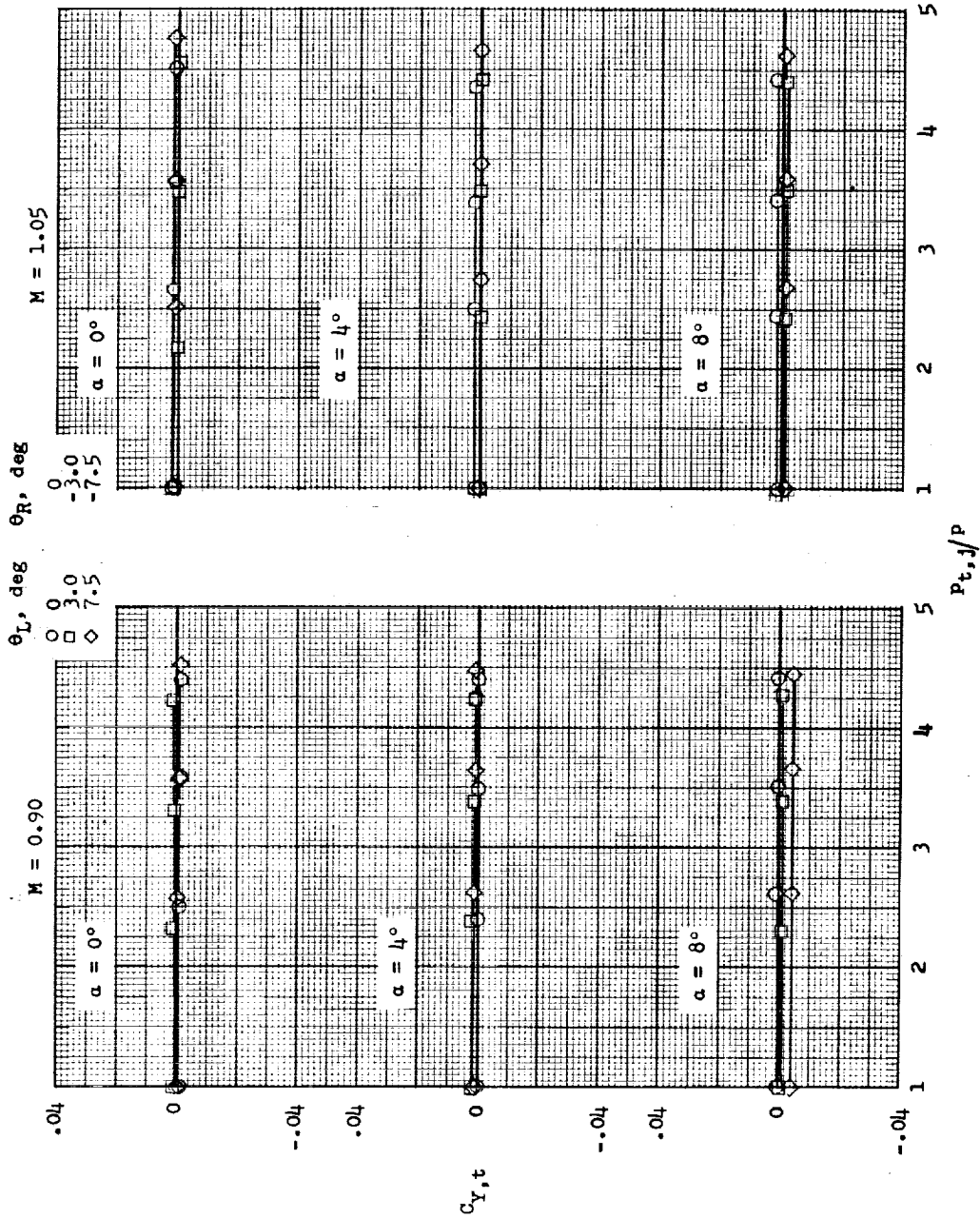
(c) Variation of rolling-moment coefficient with jet total-pressure ratio.

Figure 19.- Concluded.



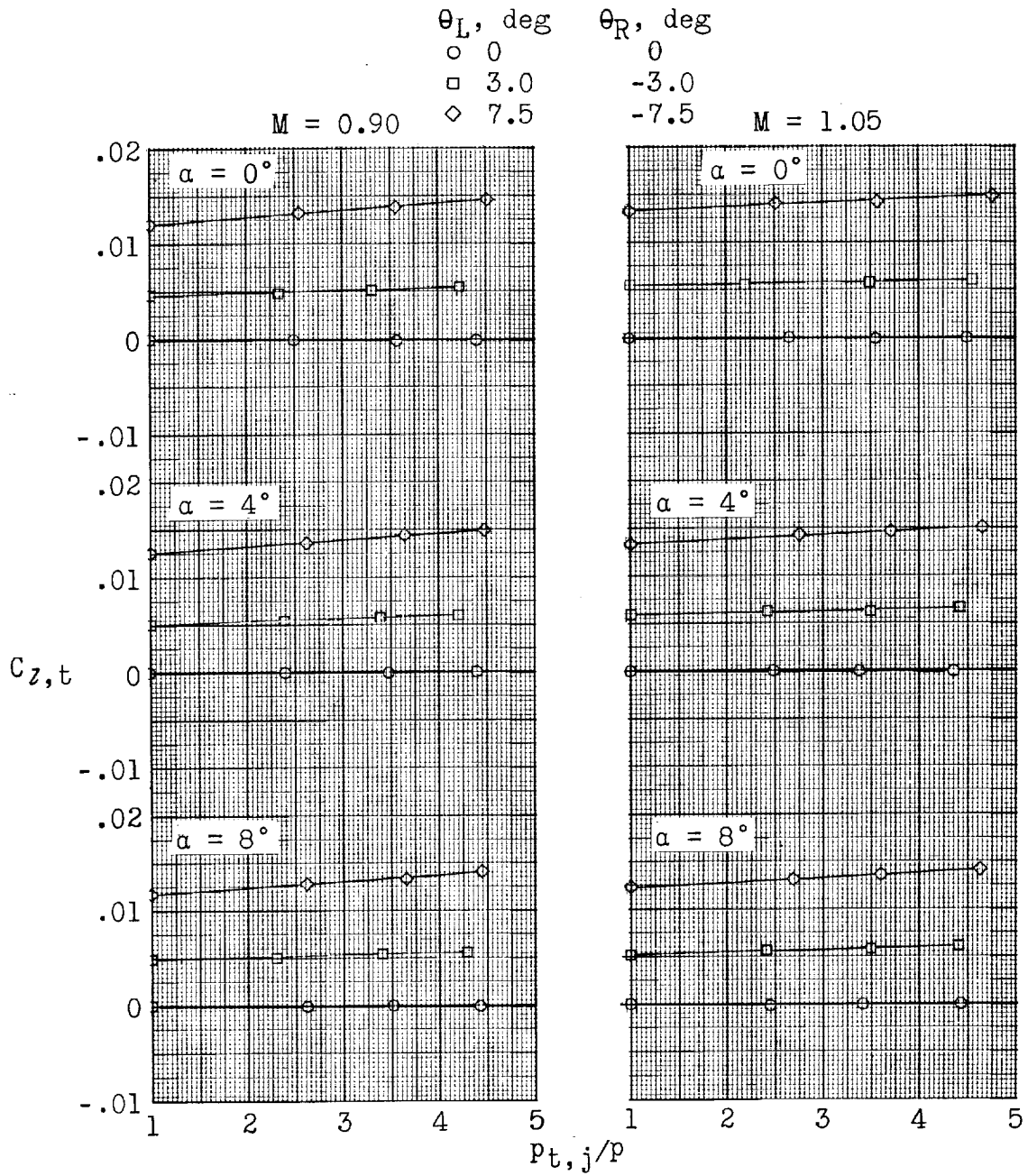
(a) Variation of yawing-moment coefficient with jet total-pressure ratio.

Figure 20.- Lateral forces and moments (including components of jet thrust) for several nacelle differential deflections in the pitch plane.



(b) Variation of side-force coefficient with jet total-pressure ratio.

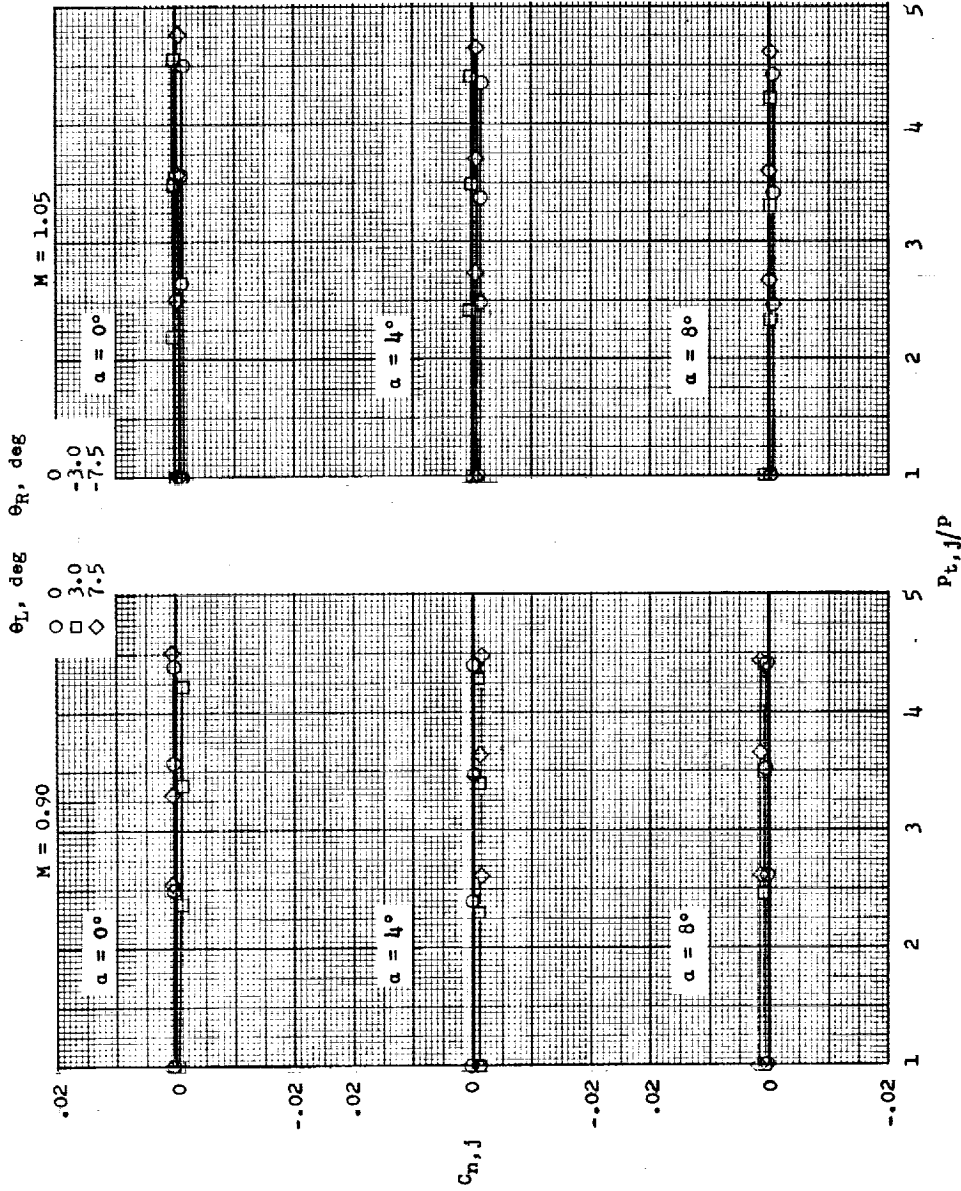
Figure 20.- Continued.



(c) Variation of rolling-moment coefficient with jet total-pressure ratio.

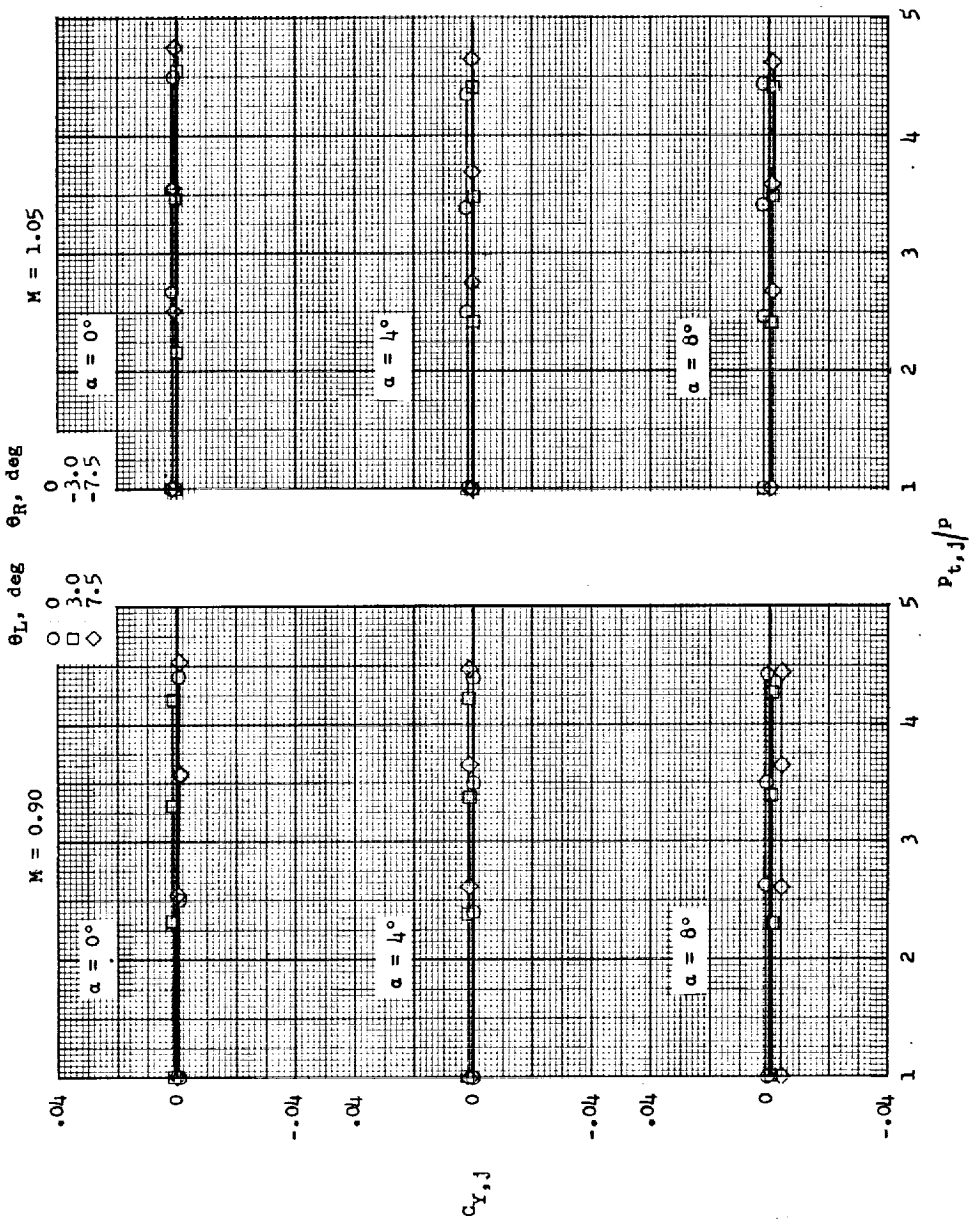
Figure 20.- Concluded.





(a) Variation of yawing-moment coefficient with jet total-pressure ratio.

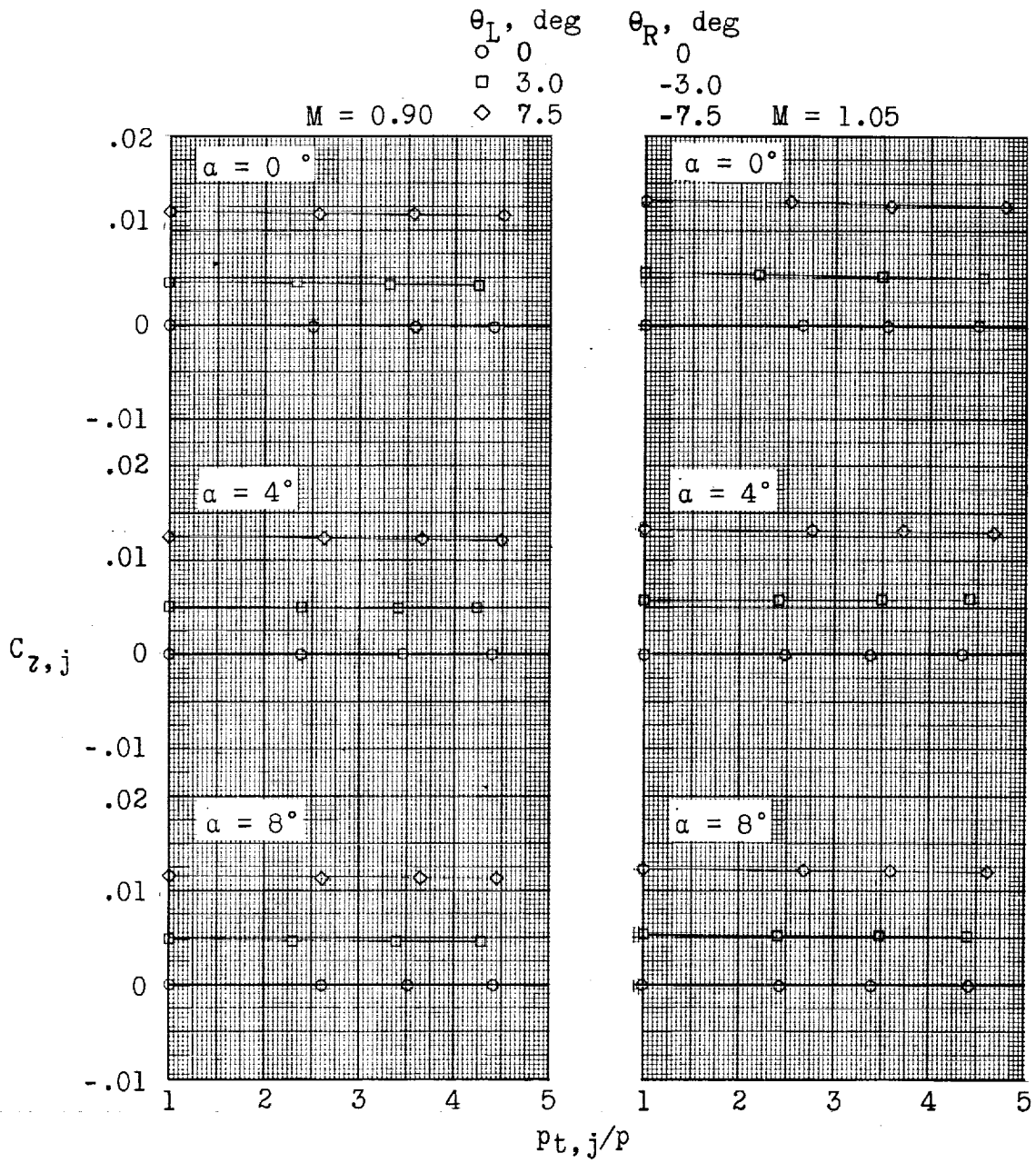
Figure 21.- Lateral forces and moments (with components of jet thrust removed) for several nacelle differential deflections in the pitch plane.



(b) Variation of side-force coefficient with jet total-pressure ratio.

Figure 21.- Continued.

SECRET



(c) Variation of rolling-moment coefficient with jet total-pressure ratio.

Figure 21.- Concluded.



SECRET

NATIONAL AERONAUTICS AND SPACE ADMINISTRATION

TECHNICAL MEMORANDUM SX-306

for the
U.S. Air Force

PERFORMANCE, STABILITY, AND CONTROL INVESTIGATION AT
MACH NUMBERS FROM 0.60 TO 1.05 OF A MODEL OF THE
"SWALLOW" WITH OUTER WING PANELS SWEPT 75°
WITH AND WITHOUT POWER SIMULATION*

By James W. Schmeer and Marlowe D. Cassetti

ABSTRACT

Four outboard engines located above and below the wing provided propulsive thrust by means of hydrogen peroxide gas generators. Deflection of the engine nacelles, which incorporated swept lateral and vertical fins, in the vertical and lateral directions also produced control forces about the three body axes. Data were obtained at angles of attack from 0° to 15° and for angles of sideslip from -5° to 10°. The results indicate that the longitudinal controls were ineffective but the directional and lateral controls were adequate. Jet interference effects on control characteristics were small; the adverse effects on drag were greater than anticipated.

INDEX HEADINGS

Wing-Nacelle Combinations - Airplanes	1.7.1.1.2
Interference, Jet-Airplane	1.7.1.1.6
Stability, Longitudinal - Static	1.8.1.1.1
Stability, Directional - Static	1.8.1.1.3
Control, Longitudinal	1.8.2.1
Control, Lateral	1.8.2.2
Control, Directional	1.8.2.3

*Title, Confidential.

~~SECRET~~

~~SECRET~~

~~SECRET~~

SECRET